nature

https://doi.org/10.1038/s41586-024-07323-1

Accelerated Article Preview

Complexity of avian evolution revealed by family-level genomes

Received: 25 April 2023

Accepted: 15 March 2024

Accelerated Article Preview

Cite this article as: Stiller, J. et al. Complexity of avian evolution revealed by family-level genomes. *Nature* https://doi.org/10.1038/s41586-024-07323-1 (2024)

Josefin Stiller, Shaohong Feng, Al-Aabid Chowdhury, Iker Rivas-González, David A. Duchêne, Qi Fang, Yuan Deng, Alexey Kozlov, Alexandros Stamatakis, Santiago Claramunt, Jacqueline M. T. Nguyen, Simon Y. W. Ho, Brant C. Faircloth, Julia Haag, Peter Houde, Joel Cracraft, Metin Balaban, Uyen Mai, Guangji Chen, Rongsheng Gao, Chengran Zhou, Yulong Xie, Zijian Huang, Zhen Cao, Zhi Yan, Huw A. Ogilvie, Luay Nakhleh, Bent Lindow, Benoit Morel, Jon Fjeldså, Peter A. Hosner, Rute R. da Fonseca, Bent Petersen, Joseph A. Tobias, Tamás Székely, Jonathan David Kennedy, Andrew Hart Reeve, Andras Liker, Martin Stervander, Agostinho Antunes, Dieter Thomas Tietze, Mads Bertelsen, Fumin Lei, Carsten Rahbek, Gary R. Graves, Mikkel H. Schierup, Tandy Warnow, Edward L. Braun, M. Thomas P. Gilbert, Erich D. Jarvis, Siavash Mirarab & Guojie Zhang

Complexity of avian evolution revealed by family-level genomes

Josefin Stiller[1]*, Shaohong Feng[2,3,4,5], Al-Aabid Chowdhury[6], Iker Rivas-González[7], David A. Duchêne[8], Qi Fang[9], Yuan Deng[9], Alexey Kozlov[10], Alexandros Stamatakis[11, 10, 12], Santiago Claramunt[13,14], Jacqueline M. T. Nguyen[15,16], Simon Y. W. Ho[6], Brant C. Faircloth[17], Julia Haag[10], Peter Houde[18], Joel Cracraft[19], Metin Balaban[20], Uyen Mai[21], Guangji Chen[9,22], Rongsheng Gao[9,22], Chengran Zhou[9], Yulong Xie[2], Zijian Huang[2], Zhen Cao[23], Zhi Yan[23], Huw A. Ogilvie[23], Luay Nakhleh[23], Bent Lindow[24], Benoit Morel[10,11], Jon Fjeldså[24], Peter A. Hosner[24,25], Rute R. da Fonseca[25], Bent Petersen[8,26], Joseph A. Tobias[27],

[1] Section for Ecology and Evolution, Department of Biology, University of Copenhagen, Denmark
[2] Center for Evolutionary & Organismal Biology, & Women's Hospital, Zhejiang University School of Medicine, Hangzhou, China
[3] Liangzhu Laboratory, Zhejiang University Medical Center, Hangzhou, China
[4] Department of General Surgery, Sir Run-Run Shaw Hospital, Zhejiang University School of Medicine, 310016, Hangzhou, China
[5] Innovation Center of Yangtze River Delta, Zhejiang University, Jiashan, China
[6] School of Life and Environmental Sciences, University of Sydney, Sydney, New South Wales, Australia
[7] Bioinformatics Research Centre, Aarhus University, Denmark
[8] Center for Evolutionary Hologenomics, The Globe Institute, University of Copenhagen, Denmark
[9] BGI-Shenzhen, Beishan Industrial Zone, Shenzhen, China
[10] Computational Molecular Evolution Group, Heidelberg Institute for Theoretical Studies, Heidelberg, Germany
[11] Institute of Computer Science, Foundation for Research and Technology Hellas, Heraklion, Greece
[12] Institute for Theoretical Informatics, Karlsruhe Institute of Technology, Karlsruhe, Germany
[13] Department of Ecology and Evolutionary Biology, University of Toronto, Toronto, Ontario, Canada
[14] Department of Natural History, Royal Ontario Museum, Toronto, Ontario, Canada
[15] College of Science and Engineering, Flinders University, Bedford Park, South Australia, Australia
[16] Australian Museum Research Institute, Australian Museum, Sydney, New South Wales, Australia
[17] Department of Biological Sciences and Museum of Natural Science, Louisiana State University, Baton Rouge, LA, USA
[18] Department of Biology, New Mexico State University, Las Cruces, NM, USA
[19] Department of Ornithology, American Museum of Natural History, Central Park West at 79th St., New York, NY, USA
[20] Bioinformatics and Systems Biology Graduate Program, University of California San Diego, La Jolla, CA, USA
[21] Computer Science and Engineering, University of California San Diego, La Jolla, CA, USA
[22] College of Life Sciences, University of Chinese Academy of Sciences, Beijing 100049, China
[23] Department of Computer Science, Rice University, Houston, TX 77584, USA
[24] Natural History Museum Denmark, University of Copenhagen, Denmark
[25] Center for Global Mountain Biodiversity, Globe Institute, University of Copenhagen, Denmark
[26] Centre of Excellence for Omics-Driven Computational Biodiscovery (COMBio), Faculty of Applied Sciences, AIMST University, Kedah, Malaysia
[27] Department of Life Sciences, Imperial College London, Silwood Park, Buckhurst Road, Ascot, SL5 7PY, UK

Tamás Székely[28,29], Jonathan David Kennedy[30], Andrew Hart Reeve[24], Andras Liker[31,32], Martin Stervander[33], Agostinho Antunes[34,35], Dieter Thomas Tietze[36], Mads Bertelsen[37], Fumin Lei[38,39], Carsten Rahbek[25,30,40,41], Gary R. Graves[42,30], Mikkel H. Schierup[7], Tandy Warnow[43], Edward L. Braun[44], M. Thomas P. Gilbert[8,45], Erich D. Jarvis[46,47], Siavash Mirarab[48]*, Guojie Zhang[2,3,5,49]*

*Corresponding authors

Correspondence to: Josefin Stiller (josefin.stiller@bio.ku.dk), Siavash Mirarab (smirarabbaygi@ucsd.edu), Guojie Zhang (guojiezhang@zju.edu.cn)

[28] Milner Centre for Evolution, University of Bath, Bath, UK
[29] ELKH-DE Reproductive Strategies Research Group, University of Debrecen, Egyetem tér 1, H-4032, Hungary
[30] Center for Macroecology, Evolution, and Climate, The Globe Institute, University of Copenhagen, Copenhagen, Denmark
[31] HUN-REN-PE Evolutionary Ecology Research Group, University of Pannonia, Veszprém, Hungary
[32] Behavioural Ecology Research Group, Center for Natural Sciences, University of Pannonia, Veszprém, Hungary
[33] Bird Group, Natural History Museum, Akeman St, Tring, Hertfordshire HP23 6AP, United Kingdom
[34] CIIMAR/CIMAR, Interdisciplinary Centre of Marine and Environmental Research, University of Porto, Porto, Portugal
[35] Department of Biology, Faculty of Sciences, University of Porto, Porto, Portugal
[36] NABU, Berlin, Germany
[37] Centre for Zoo and Wild Animal Health, Copenhagen Zoo, Frederiksberg, Denmark
[38] Key Laboratory of Zoological Systematics and Evolution, Institute of Zoology, Chinese Academy of Sciences, Beijing 100101, China
[39] College of Life Science, University of Chinese Academy of Sciences, Beijing 100049, China
[40] Institute of Ecology, Peking University, Beijing 100871, China
[41] Danish Institute for Advanced Study, University of Southern Denmark, Odense 5230, Denmark
[42] Department of Vertebrate Zoology, National Museum of Natural History, Smithsonian Institution, Washington, DC, USA
[43] University of Illinois Urbana-Champaign, Champaign, IL, USA
[44] Department of Biology, University of Florida, Gainesville, FL 32611, USA
[45] University Museum, NTNU, Trondheim, Norway
[46] Vertebrate Genome Lab, The Rockefeller University, New York, NY, USA
[47] Howard Hughes Medical Institute, Durham, NC, USA
[48] University of California, San Diego, San Diego, CA, USA
[49] Villum Center for Biodiversity Genomics, Department of Biology, University of Copenhagen, Copenhagen 2100, Denmark

Summary

Despite tremendous efforts in the past decades, relationships among main avian lineages remain heavily debated without a clear resolution. Discrepancies have been attributed to diversity of species sampled, phylogenetic method, and the choice of genomic regions [1–3]. Here, we address these issues by analyzing genomes of 363 bird species [4] (218 taxonomic families, 92% of total). Using intergenic regions and coalescent methods, we present a well-supported tree but also a remarkable degree of discordance. The tree confirms that Neoaves experienced rapid radiation at or near the Cretaceous–Paleogene (K–Pg) boundary. Sufficient loci rather than extensive taxon sampling were more effective in resolving difficult nodes. Remaining recalcitrant nodes involve species that challenge modeling due to extreme GC content, variable substitution rates, incomplete lineage sorting, or complex evolutionary events such as ancient hybridization. Assessment of the impacts of different genomic partitions showed high heterogeneity across the genome. We discovered sharp increases in effective population size, substitution rates, and relative brain size following the K–Pg extinction event, supporting the hypothesis that emerging ecological opportunities catalyzed the diversification of modern birds. The resulting phylogenetic estimate offers novel insights into the rapid radiation of modern birds and provides a taxon-rich backbone tree for future comparative studies.

Main

Understanding the evolutionary relationships among species is fundamental to biology, not only as an account of speciation events, but also as the basis of comparative analyses of trait evolution. However, for deep phylogenetic relationships, different studies often reveal incongruence across analyses [5,6]. Large amounts of data may be required to resolve certain relationships, yet others can remain recalcitrant even with genome-scale efforts, particularly for rapid radiations [7,8]. Phylogenomic incongruence can point to statistical and systematic errors but is also increasingly linked to complex biological processes that accompany rapid diversification [9,10]. Prime examples of this problem are the phylogenetic relationships among modern birds (Neornithes), which are inconsistently resolved even with large-scale datasets [1–

[3,11]. The widespread incongruences in evolutionary histories across avian genomes [1,12,13] has left the phylogenetic relationships of major extant groups unclear and possibly irresolvable [14].

Modern birds comprise three major groups: ratites and tinamous (Palaeognathae), landfowl and waterfowl (Galloanseres), and all other living birds (Neoaves). The early Neoaves experienced a rapid diversification into at least ten major clades [15], the so-called "magnificent seven" and three "orphans" [12], encompassing 95% of extant species and a significant portion of their phylogenetic diversity. Due to the short internal branches between these clades, their relationships remain contentious [1–3,16]. Further, the timing of the radiation of these major groups is debated [17,18]. The 'mass survival' scenario places the radiation before the K–Pg mass extinction (66.043 ± 0.011 Ma [19]), requiring survival of multiple neoavian lineages through the global changes caused by the Chicxulub impact [11,17,20]. The alternative 'big bang' scenario implies a rapid diversification of neoavian groups following the mass extinction, driven by adaptive radiation into new habitats and in the absence of competitors [21]. Fossil evidence supports the scenario of morphological diversification following the K–Pg event [22]. Several molecular studies also supported rapid divergences [1–3], yet wide credible intervals (CI) allowed for the possibility that some of the earliest neoavian divergences predated the K–Pg boundary [23]. Uncertain placement of key taxa and a wide range of time estimates also persist within Passeriformes, the largest avian order with over 6000 living species [3,24].

Efforts to resolve the high level avian phylogeny face two major challenges. First, it is difficult to obtain large numbers of orthologous loci with suitable properties for phylogenetic analyses. Many studies have been limited to conserved genomic regions such as protein-coding sequence (exons) and ultraconserved elements (UCEs) [2,25]. Conserved regions exhibit complex patterns of sequence evolution; for example, selection to maintain protein structure and function places constraints on exon evolution [12]. Standard models of sequence evolution practical for large datasets exhibit poor fit to these regions, and model misspecifications likely result in topological discrepancies across data types [1,12,13]. Analyzing large numbers of loci does not remove, but can instead reinforce, biases introduced by model violations [1,7]. In principle, data types under lower selective pressure such as introns and intergenic regions are preferable. Intergenic regions are arguably ideal because they are less likely under strong selection [13]. The second challenge is collecting genomic data from sufficient numbers of species, given that dense taxon sampling can improve phylogenetic estimation [26,27]. Thus, the debate in avian phylogenetics has revolved around the trade-off between using diverse loci

extracted from entire genomes but for few species (one genome per taxonomic order) [1] or using a smaller number of potentially biased loci sampled from more species [2,3]. Both approaches have shortcomings. The most compelling solution is also the most challenging: to create comprehensive datasets with whole genomes sampled across many taxa that inform on deeper timescales.

Here, as one of the main missions of the 'family phase' of the Bird 10K Genomes project [28], we generated a phylogeny for modern birds by sampling across genome assemblies of 363 species representing 218 families (92% of the total) [4] (Supplementary Data). We analyzed nearly 100 billion nucleotides (~275 Mb for each species, Extended Data Fig. 1a), an alignment 50 times the size of the largest available dataset of 48 species [1] (Extended Data Fig. 1b). As our main data source, we used evenly spaced sampling of intergenic regions across 10 kb windows of a whole genome alignment [4] (Extended Data Fig. 1c). We found that selecting a 1-kb locus within the first 2 kb of each window balanced phylogenetic informativeness against including recombination within loci (Extended Data Fig. 1d, Methods). This resulted in 94,402 1-kb loci, from which we removed loci that overlapped with exon and intron regions, resulting in a set of 63,430 purely intergenic loci (total 63.43 Mbp). In addition to analyzing this main set, we test the impact of various factors, including adding introns and exons, describe the major sources of phylogenetic incongruence, and identify the remaining cases of uncertainty.

Intergenic regions resolve deep branches

Our main phylogenetic tree (called 'main tree') was obtained by analyzing the 63k intergenic loci within a coalescent-based framework (Fig. 1, Extended Data Fig. 2, Extended Data Fig. 3). We focus on this tree because the findings reported below show that intergenic regions reduce systematic error due to model misspecifications – results that match *a priori* expectations and previous analyses [12,29]. The use of a coalescent-based method [30,31] accounts for well-documented incomplete lineage sorting (ILS) in early Neoaves [1,32]. A concatenated analysis of the same 63k loci (Extended Data Fig. 4) resulted in a similar tree that differed in only 10 of the 360 branches (2.8%). In these topologies, 98.1% of nodes had full statistical support (main tree: 3 nodes <1.00 posterior probability (PP); concatenation: 7 nodes <100% bootstrap support). While our main topology differed from those of all previous studies, it was more similar to the genome-wide 'TENT' tree from Jarvis et al. [1]of 48 species, than to

the main topology from Prum et al. [2], which was based on mostly protein-coding genes of 198 species (Extended Data Fig. 5).

Within Neoaves, we resolve four major clades (Fig. 1a). Three of these are Mirandornithes (grebes and flamingos), Columbaves (Columbimorphae [doves, sandgrouse, and mesites] and Otidimorphae [cuckoos, bustards, and turacos]), and Telluraves (higher landbirds including Afroaves and Australaves). The fourth major clade is new and phenotypically diverse, containing Aequornithes (pelicans, tubenoses, penguins, and loons), Phaethontimorphae (kagu, sunbittern, and tropicbirds), Strisores (nightbirds, swifts, and hummingbirds), Opisthocomiformes (hoatzin), and Cursorimorphae (shorebirds and cranes). This clade was supported in coalescent-based analyses of the intergenic regions, and UCEs, but not by the exons, introns, or in concatenated analysis of the intergenic regions (Fig. 3d, Extended Data Fig. 4). We name the clade Elementaves because its lineages have diversified into terrestrial, aquatic, and aerial niches, corresponding to the classical elements of earth, water, and air, and several Phaethontimorphae have names derived from the sun, representing fire.

Most Neoaves diversified post-K–Pg

To time-calibrate our main tree, we empirically generated calibration densities for 34 nodes using 187 fossil occurrences (Supplementary Information) and applied these in a Bayesian sequential subtree framework (Methods). We estimated branch lengths from intergenic regions and excluded loci that had evolved at the lowest and highest rates, and those with the greatest rate variation across lineages. Our analysis produced age estimates with 95% CI that were considerably narrower than previously achieved (Extended Data Fig. 6a). The widest CI were observed for nodes positioned farthest from the calibration points, including the secondary calibrations involved in subtree dating. The prospects for narrowing the intervals are promising through future refinement and addition of fossil-based age constraints. In contrast with a recent study proposing a diversification of Neoaves during the Upper Cretaceous [11], we found that the early divergences in Neoaves were tightly associated with the K–Pg boundary (Fig. 1b). Only two divergences occurred before the boundary: Mirandornithes diverged from the remaining Neoaves 67.4 Ma ago (95% CI 66.2–68.9), and Columbaves diverged 66.5 Ma ago (95% CI 65.2–67.9). All subsequent divergences postdate the boundary, although the 95% CI of the divergence time between Telluraves and Elementaves and the crown age of Elementaves span the K–Pg boundary. This evolutionary

timeline, wherein only a few neoavian lineages diverged before the K–Pg event, is reflected in all alternative dating analyses (Methods, Extended Data Fig. 6b-e), highlighting the robustness of our estimated chronology. This lends more support to a post-K–Pg diversification of Neoaves than previous studies, where the 95% CI of 10 to 18 of the nodes allowed for pre-K–Pg divergences [1,2,18,23].

Abundant discordance among gene trees

Assessing the level of incongruence between gene trees across the main tree, order-level relationships ranged from showing little or no discordance to high levels of discordance (measured by the quartet score, Fig. 2a). The percentage of gene tree quartets matching a species tree branch at the ordinal level ranged from 99.9% to 33.7% (close to ⅓, which corresponds to a polytomy). In particular, 14 nodes had quartet support below 37%. These are the same nodes that have been difficult to resolve in past studies [15]. For 29 out of 33 nodes, the quartet support of the main topology was significantly higher than the two alternatives (one-sided $\chi 2$ test with BH multiple test correction), consistent with expectations under ILS models. We discuss the remaining nodes (26, 39, 43, 49 in Fig. 2b) below.

Mirandornithes is sister to other Neoaves

The placement of Mirandornithes (also called Phoenicopterimorphae [33]) as the sister lineage to the remaining Neoaves was supported by both the main tree and concatenation. Although this topology was reported previously [3], it differs from the TENT tree of Jarvis et al. [1], which grouped Mirandornithes and Columbimorphae into a clade called Columbea. In the main tree, Columbimorphae combined with Otidimorphae to form Columbaves. This clade has also been reported previously, albeit with low bootstrap support [2]. Mirarab et al. [34] showed that a 21 Mb outlier region of chromosome 4 with abnormally strong signal for Columbea (potentially due to effects of ancient interchromosomal rearrangements) is responsible for the previous recovery of Columbea. However, with additional taxon sampling of Otidimorphae and Columbimorphae, the impact of this outlier region gradually lessened in favor of an increasingly dominant signal from the remaining genome that placed Mirandornithes as the sister to other Neoaves (Extended Data Fig. 7a). In the concatenated analysis, Mirandornithes and Columbimorphae weare successive sister groups to Otidimorphae and remaining clades but with limited support (BS=64, Extended Data Fig. 4). Finally, when analyzing exons,

Mirandornithes were placed deeper in Neoaves as sister to Aequornithes+Phaethontiformes (Extended Data Fig. 4), which may relate to previous association with mostly aquatic birds in studies analyzing large portions of coding regions (sister to Charadriiformes [2], Opisthocomiformes+Aequornithes+Phaethontimorphae [11]).

There is a rapid succession of nodes in this part of the tree, with only 0.92 Ma between the divergence of Mirandornithes and of Columbaves from other groups. Within Columbaves, Otidimorphae has been found in some studies [1,2], but not in others [3,12]. Within Otidimorphae, we resolved Otidiformes as the sister group to Cuculiformes like some [12] but unlike several other studies [1–3]. The difficulty could be explained by the very short branch (0.57 Ma) separating Otidiformes and other Otidimorphae. Similarly, Columbiformes diverged from the remaining Columbimorphae within 0.26 Ma. These fast divergences partially explain why previous analyses with less data led to conflicting resolutions of these earliest neoavian branches.

Waterbirds are deep in a diverse clade

Unlike previous hypotheses that placed Phaethoquornithes (Aequornithes+Phaethontimorphae) as sister to landbirds [1,3], the main tree placed Phaethoquornithes deep inside the diverse Elementaves (Fig. 1a). The "orphans" Charadriiformes and Gruiformes were consistently grouped together (forming Cursorimorphae), as found in some other studies [1,3]. The placement of the third orphan, Opisthocomiformes, as the sister to this group (with a short branch of 0.58 Ma) was the sole instance across the entire phylogeny with statistically indistinguishable levels of gene tree support for all three possible configurations around this branch [35] (Fig. 2b), a noteworthy finding given the extensive amount of available data.

Conflict among early Elementaves

While the main tree placed Phaethontimorphae as the sister to Aequornithes, further investigations revealed a competing placement as the sister lineage to Telluraves. Both topologies have been previously reported [1–3,12], with their difference attributed to the effects of using protein-coding (Phaethontimorphae+Aequornithes) versus non-coding regions (Phaethontimorphae+Telluraves) [15]. We found instead that both topologies have support in

the intergenic data. While Phaethontimorphae+Aequornithes had a slightly better quartet score, it was recovered in only 60% of trees resulting from randomly subsampling half of the 63k loci (Extended Data Fig. 7b). The two alternative positions of Phaethontimorphae, which are three branches (9.1 Ma) away, each had full local support (PP=1.0). Yet, global bootstrap support estimated from resampling gene trees revealed uncertainty in the three nodes connecting the two placements (globalBS=42–62, Fig. 2b). Two hypotheses could explain this non-local uncertainty. One is ancient hybridization between ancestral Phaethontimorphae and Telluraves, 3.96 Ma after their divergence. Alternatively, the high support for the alternative placement could be due to problems arising from long branches. Phaethontimorphae have ~25% longer terminal branches than Aequornithes (paired t-test across loci, $p<2.2\times10^{-16}$), showing greater similarity to Telluraves in this regard (Fig. 2b). Consistent with this explanation, topological changes resulted from data filtering that targeted long branches (clocklikeness, stemminess, total coverage, tree length, Extended Data Fig. 7c).

Our main tree placed Strisores (also called Caprimulgiformes [33]) with Phaethoquornithes with moderate support (PP=0.90, Fig. 1a), while the concatenated tree grouped them as sister to Telluraves with low support (BS=32, Extended Data Fig. 4). Quartet frequencies did not follow an ILS-alone scenario, as moving Strisores to the base of Elementaves had quartet frequencies similar to the main tree (χ^2 test, $p_{BH\ adjusted}=0.317$), while the third alternative had lower frequency ($p=0.488\times10^{-11}$). Possible explanations include hybridization or long branch attraction because Strisores have 4–28% longer branches than the other Elementaves, which may attract them to the long-branched Telluraves (Fig. 2b). Previous studies also failed to find unequivocal support for the relationship of Strisores, placing it as sister to Otidimorphae [1], Cursorimorphae [11], Opisthocomiformes [3], or all other Neoaves [2]. Within Strisores, our tree positioned Caprimulgidae (nightjars), instead of Sedentaves (oilbird+potoos) [12], as sister to all others (Extended Data Fig. 2), as found before [2,11].

Difficult placement of owls and hawks

Within Telluraves, our main tree supported the proposed split into Australaves and Afroaves [1,3] in contrast to other studies [2,11]. Our tree grouped Accipitriformes and Strigiformes as the sister to the remaining Afroaves, similar to previous coalescent-based analyses [1].

Concatenated analyses [1,3], including ours, supported Accipitriformes alone as sister to the remaining Afroaves (Extended Data Fig. 4). This node also showed quartet frequencies that were statistically indistinguishable for two topologies (35% vs. 34.6%, χ^2 test, $p_{BH\ adjusted}$=0.130), while the third was significantly lower (30.5%, $p<10^{-16}$; node 26 in Fig. 2b), contradicting expectations of ILS. Since we found no evidence of long branch attraction (Extended Data Fig. 7d), the non-ILS patterns could be indicative of ancestral hybridization [36]. In contrast to gene trees, direct analysis of alignment sites using CoalHMM (Methods) supported an ILS-like pattern, where the two alternative topologies had similar scores (31.2% vs. 29.6%). However, CoalHMM assumes ILS *a priori* and only a strong signal of hybridization can lead to inferring unbalanced quartet frequencies. Thus, an ancestral hybridization event, albeit too weak to be detected by CoalHMM, remains plausible. Additionally, we observed that the relationship between Accipitriformes and Strigiformes depended on the number of passeriform taxa sampled. The main topology was obtained only when at least 138 Passeriformes were included, whereas sampling fewer taxa of each order favored Accipitriformes as the sister to the remaining Afroaves (Fig. 2c). This case demonstrates that the impact of taxon sampling of one group can extend to others and that these sampling effects are not easily predictable.

Insights into the passerine radiation

Our analyses of phylogenetic relationships among Passeriformes (perching birds) included 173 species in 121 families and seven fossil calibrations. The most recent common ancestor of Passeriformes was dated to 50.7 Ma (95% CI 48.3–53.0, Fig. 1). This estimate is broadly similar to those from other studies with broad taxon sampling (47–53 Ma [2,3,23,24]), while a previous genomic study that included only five passeriforms found a considerably younger age (39 Ma [1]). The split between Tyranni (Suboscines) and Passeri (Oscines) was estimated at 47.3 Ma (95% CI 45.1–49.8, Extended Data Fig. 3), in line with a previous study [2], but 3–4 Ma older than other estimates [3,24]. Tyranni and Passeri were estimated to have started diversifying around the same time, while other studies supported a 3 Ma difference between the onset of their diversification [2,3]. The three main clades of Tyranni (Eurylaimides, Tyrannides, and Furnariides) were inferred to be 4–12 Ma younger than previously found [37]. In Passeri, the age of Corvides was estimated to 25.7 Ma (95% CI 23.8–27.7), agreeing with some previous estimates [24], but over 5 Ma younger than others [3]. The divergence of a major subclade of Passerides (Sylviida+Muscicapida+Passerida) was inferred to have occurred

shortly after the Paleogene–Neogene boundary (22.4 Ma, 95% CI 20.6–24.2, Extended Data Fig. 3), while previous studies placed its divergence before the boundary [3,23,24]. This branch and some subsequent divergences occurred in close succession, indicating a rapid diversification.

In Passeri, our tree differed from studies based on UCEs or 5′-UTR sequences [3,24,38], including the positions for Orioloidea, Malaconotoidea, Corvoidea, Mohouidae, Neosittidae, Regulidae, and Urocynchramidae (asterisks in Fig. 3d, Supplementary Information). Some of these difficulties also appear to be related to fast diversification, seen for example in the extremely short internode (0.18 Ma) of Mohouidae.

Rheas have conflicting placements

Outside of Neoaves, we found support for different relationships of Rheiformes within Palaeognathae, a conflict previously attributed primarily to ILS [39]. While our main topology found Rheiformes as the sister to Tinamiformes, analysis with CoalHMM put it as sister to Apterygiformes+Casuariiformes (Extended Data Fig. 7g), in agreement with the previous study [39]. We found that Rheiformes and Tinamiformes had a higher proportion of loci with high GC content than other taxa (Extended Data Fig. 7e). We observed that omitting loci with similar GC content for Tinamiformes and Rheiformes, but not for others, tended to reduce (but not eliminate) support for this clade (Extended Data Fig. 7g). These results suggest that the strong support for this grouping in our main tree was enhanced by biased GC content, leaving other placements of Rheiformes (e.g., as sister to Apterygiformes+Casuariiformes, as recovered by CoalHMM) plausible.

Impact of taxon sampling varies

The question of whether to sample more species or more genetic loci is pivotal for phylogenetic study design [40]. While expanding taxon sampling helps mitigate the confounding impact of long branches within gene trees [26,41], its effects on species tree inference are less clear. To investigate this question, we randomly selected 1 to 10 species for each order and constrained the 63k intergenic gene trees to the selected taxa before rescoring the species tree. These changes in taxon sampling affected ordinal relationships in only three cases (Extended Data Fig. 7f), with the aforementioned Accipitriformes+Strigiformes being the strongest example (Fig. 2c). More frequently, we observed that increasing taxon sampling

affected only the amount of gene tree discordance but not the topology (e.g., Telluraves+Elementaves in Fig. 2c). Thus, our results are relatively robust to taxon sampling, though with some exceptions.

Number of loci needed vary across nodes

As access to large numbers of loci becomes common, the choice of how many and which loci to select isa fundamental decision [42]. Using repeated subsets of the 63k dataset, we found that greater locus sampling resulted in trees more similar to the main tree and with higher support (Fig. 3a). The same trend was observed across all partitions of the genome (intergenic regions, introns, UCEs, and exons; Extended Data Fig. 8ab) and with other species trees as reference, except the purely exonic one (Extended Data Fig. 8c).

We assessed how many loci were required to consistently recover each clade of the main tree (Fig. 3b). We found that most clades (321/361, 89%) could be identified with just 1000 loci. A minority of clades (30/361, 8%) needed substantially more, from 2000 to 32,000 loci, before analyses could consistently support them (Fig. 3c). In the remaining 10 clades (2.8%), increasing the number of loci reduced incongruence but did not consistently recover the main topology across replicates, even with 32,000 loci (Fig. 3c, Extended Data Fig. 9). Most of these difficult nodes were associated with short branches after the K–Pg boundary and within Corvides (Fig. 3b). For example, the mousebirds (Coliiformes), placed in agreement with some studies [1–3] in our main tree, had an alternative placement in 30% of subsets of 32,000 gene trees, consistent with previously reported difficulties [1,14].

Strong impacts of different locus types

Species trees built from gene trees of different data types were substantially different, especially between protein-coding and non-coding data, akin to previous findings [1,12,13]. The species tree built from 14k exon loci (excluding the hypervariable third codon position) differed in 38/360 branches from the main tree (compared with 6–7 differences for the other data types, Extended Data Fig. 4). Beyond dissimilarity to the main tree (Fig. 3d), trees inferred from exons were less internally consistent: they were more sensitive to subsampling than trees built from other data types (Extended Data Fig. 8a-c). Even when controlling for the number of gene trees used in species tree construction, exons produced more variable trees than other data types (Fig. 4a).

We found that data types differed in the risk of violating assumptions of phylogenetic models. A much higher proportion of exonic loci were found to be at risk of sequence saturation (30.83%) compared to the other data types (intergenic regions: 0.07%, UCEs: 0.34%, introns: 0.83%). The evidence for violating stationarity was generally low, yet highest among exons (exons: 2.45% of loci failing the test, UCEs: 0.02%, intergenic regions: 0.07%, introns: 0.08%). Moreover, because individual exons of the same gene were joined into one locus, the assumption that phylogenetic loci are recombination-free is expected to be more frequently violated by exonic loci. An exonic locus can span wide stretches of the genome because its individual exons are not contiguous (mean sequence length=16,964 bp, range=149-566,199), as opposed to loci of other data types (mean sequence length, intron: 2543 bp, UCEs: 2095 bp, intergenic regions: 897 bp). The increased length of exons increases the risk of within-locus recombination. Thus, analyzing only intergenic regions minimizes the risk of recombination and model violations.

We found that exonic loci had less phylogenetic information and were more variable in their signal than the other data types (Extended Data Fig. 8d-e). Exons also scored highest in a measure of phylogenetic estimation difficulty (Extended Data Fig. 8f), indicating that their gene trees are less reliable than those of other data types. To examine if exons had misleading signal, we restricted species tree inference to gene trees with more signal, less gappy alignments, greater clocklikeness, and greater total length. Unlike intergenic regions, where subsampling did not systematically change the species trees, using more informative, less gappy, and more clocklike exons reduced the incongruence between the resulting species trees and the main tree (Fig. 4b; Extended Data Fig. 8g). Thus, exons yield phylogenetic trees that are less reliable. This conclusion is consistent with earlier analyses based on fewer genomes [1,12,13,29]. Our results indicate that the damaging effects of model violation and limited signal of exons are not offset by increased taxon sampling, as one might hope [2,43].

In order to investigate whether the confounding effects of exons could be swept out by other data, we gradually augmented the purely intergenic loci (Extended Data Fig. 1b). Adding 1 kb windows that overlapped with introns (resulting in a total of 86k loci) led to the same topology. However, when windows overlapping with exons were added (94k loci), the resulting tree agreed with the main tree on the first four neoavian clades (Mirandornithes, Columbaves, Telluraves, and Elementaves), but differed in five difficult branches (Fig. 3d,

Extended Data Fig. 4). This 94k topology was also obtained when adding the UCEs, purely intronic loci, and purely exonic loci (not those overlapping with 1 kb windows) to either the 63k set (128k loci) or the 94k set (159k loci). Removing loci that failed saturation and stationary tests from the full set (153k loci left) returned the same tree, albeit with low support on branches conflicting with the main tree (Fig. 3d). These results indicate that the inclusion of exonic loci, even if they constitute just 10% of the data and restricted to those that pass tests of model fit, can impact the most unstable parts of the tree. This finding can partially explain the different topologies reported in other studies using a high proportion of coding regions [2,11]. In contrast, exclusion of introns did not make a difference topologically in our analyses. Nevertheless, we treat the five branches that differ between purely intergenic regions and these alternative trees as uncertain.

Discordance along chromosomes

Averaged over 500 kb windows, gene discordance levels were mostly consistent along chromosomes (31.4% normalized Robinson-Foulds distance to the main tree, Fig. 4c). However, we observed some notable troughs and peaks of gene tree discordance, particularly around the telomeres and some centromeres (relative to the chicken genome), agreeing with prior findings regarding telomeres [1]. Gene trees inferred from macrochromosomes (>50 Mb) were slightly less distant to the main tree than intermediate chromosomes (12–40 Mb) and microchromosomes (average size 12 Mb, Extended Data Fig. 10a). The higher discordance near telomeres and across microchromosomes may be related to their elevated richness of genes, GC content variation, and higher recombination rates (Fig. 4c, Extended Data Fig. 10b-d) leading to higher local effective population size and challenging phylogenetic reconstruction. The Z chromosome had the lowest discordance (Extended Data Fig. 10a), consistent with its lower recombination rate. Species trees inferred from individual chromosomes resulted in topologies with 1–3% difference to the main tree, with most differences observed in microchromosomes followed by intermediate chromosomes (Extended Data Fig. 10a).

Implications for avian diversification

We next evaluated how well the new phylogenetic tree reflects avian morphology, testing the expectation that closely related species should resemble one another. We found that our main tree fits morphological traits better than the Prum et al. [2] topology, even when controlling for taxon sampling (Fig. 5a), including the larger number of Passeriformes in our study (Supplementary Results in Supplementary Information). Simulations considering the misplacement of taxa and convergent scenarios suggested that the higher phylogenetic signal in this comparison was more likely attributed to topological differences (Extended Data Fig. 11a).

Next, we compared branch lengths in time units and coalescent units,, which should be proportional to population size, ignoring the impact of varying generation time (Methods). We found a strong signal of increased population sizes on nearly half of the branches 0–2 Ma after the K–Pg transition (Fig. 5b), agreeing with an earlier analysis of insertions and deletions [44]. This pattern could be indicative of lineages undergoing density compensation, a transient increase in population size in response to ecological opportunity and release that may be associated with adaptive radiation [45]. Birds would have been well-positioned to exploit landscapes newly devoid of competitors and predators following the K–Pg mass extinction because of their flight capabilities. Vagile insectivores and marine species such as Strisores and Aequornithes could have rapidly expanded into early-succession habitats. A less dramatic spike was also observed around the end of the Paleogene (Fig. 5b). There was also an apparent gradual decline in the ratio of time and coalescent unit branch lengths by close to an order of magnitude over 60 Ma. A reduction in generation times could plausibly produce this result, possibly reflecting an increase in numbers of passerine families through time. There has also been a trend toward reduced inferred body sizes over this time (Fig. 5c), and it has long been appreciated that taxa with small body size have short generation times [46].

Substitution rate estimates for the intergenic regions also showed a strong increase at and shortly after the K–Pg boundary (Fig. 5d), and a more diffuse increase near the boundary to the Neogene. The rate increase near the K–Pg boundary has been noted for other data types and attributed, at least in part, to the "Lilliput effect" [47,48]. It refers to decreases in body size in the wake of mass extinctions; those changes in body size would affect other life history traits, such as generation time. Consistent with this explanation, we found a decrease in

reconstructed body size after the K–Pg event (Fig. 5c). This was accompanied by an increase in inferred relative brain size shortly before the K–Pg event, suggestive of strong selection for adaptability or behavioral flexibility, consistent with previous findings [49]. Shortly after the K–Pg event, the continuous changes of inferred relative brain size appear to have ceased (Fig. 5c). From ~35 Ma, the reduction in reconstructed body mass does not seem to have been accompanied by an increase in relative brain size.

Across the tree, we found that rapid evolutionary change occurred at the origin of major clades, throughout the diversification of some clades, and along some isolated branches. Passeriformes exhibited a burst of body mass evolution at their most recent common ancestor (Extended Data Fig. 11b). Rates of evolution in relative brain size were more variable, with rapid evolutionary change in some clades (e.g., Telluraves, vocal learning lineages such as parrots, corvids, and hummingbirds)[49]. Additionally, our data showed that the early burst was followed by sustained varied rates within these groups, especially in Passeri (Extended Data Fig. 11c).

Conclusions

Relationships along the backbone of Neoaves have long been contentious, with various analyses yielding incongruent results. At the heart of the disagreements has been a long-standing question: Is it better to sample many taxa at a few loci (typically conserved regions, such as exons and UCEs) or sample many loci widely across the genome, even if available from fewer species? We can finally answer this question because our data provide both dense taxon sampling and many loci across the whole genome. We observed that the number of loci, in addition to sequence types (e.g., exon, intron, intergenic regions, or chromosome type), had a much greater effect on the inferred tree than taxon sampling. Nevertheless, increased taxon sampling was crucial in inferring more precise dates, and for studying traits, trajectories of population size and substitution rates. By focusing on intergenic regions, a source of data that has been largely unused in the past, we minimized model violations and increased phylogenetic resolution. Yet, our results also showed that several recalcitrant relationships remain, even with this wealth of data, due to challenges imposed by biological processes such as hybridization that are hard to model in deep time using phylogenetics.

Overall, our results underscore the complexity of genome evolution and reveal methodologies that are likely to be useful for future phylogenomic studies focused on deep relationships.

References (main text)

1. Jarvis, E. D. *et al.* Whole-genome analyses resolve early branches in the tree of life of modern birds. *Science* **346**, 1320–1331 (2014).
2. Prum, R. O. *et al.* A comprehensive phylogeny of birds (Aves) using targeted next-generation DNA sequencing. *Nature* **526**, 569–573 (2015).
3. Kuhl, H. *et al.* An unbiased molecular approach using 3'-UTRs resolves the avian family-level Tree of Life. *Mol. Biol. Evol.* **38**, 108–127 (2021).
4. Feng, S. *et al.* Dense sampling of bird diversity increases power of comparative genomics. *Nature* **587**, 252–257 (2020).
5. Hinchliff, C. E. *et al.* Synthesis of phylogeny and taxonomy into a comprehensive tree of life. *Proc. Natl. Acad. Sci. U. S. A.* **112**, 12764–12769 (2015).
6. One thousand plant transcriptomes and the phylogenomics of green plants. *Nature* **574**, 679–685 (2019).
7. Jeffroy, O., Brinkmann, H., Delsuc, F. & Philippe, H. Phylogenomics: the beginning of incongruence? *Trends Genet.* **22**, 225–231 (2006).
8. Philippe, H. *et al.* Resolving difficult phylogenetic questions: why more sequences are not enough. *PLoS Biol.* **9**, e1000602 (2011).
9. Schrempf, D. & Szöllősi, G. The sources of phylogenetic conflicts. *Phylogenetics in the Genomic Era* 3.1:1–3.1:23 (2020).
10. Bravo, G. A. *et al.* Embracing heterogeneity: coalescing the Tree of Life and the future of phylogenomics. *PeerJ* **7**, e6399 (2019).
11. Wu, S. *et al.* Genomes, fossils, and the concurrent rise of modern birds and flowering plants in the Late Cretaceous. *Proc. Natl. Acad. Sci. U. S. A.* **121**, e2319696121 (2024).
12. Reddy, S. *et al.* Why do phylogenomic data sets yield conflicting trees? Data type influences the

avian Tree of Life more than taxon sampling. *Syst. Biol.* **66**, 857–879 (2017).

13. Braun, E. L. & Kimball, R. T. Data types and the phylogeny of Neoaves. *Birds North America* **2**, 1–22 (2021).

14. Suh, A. The phylogenomic forest of bird trees contains a hard polytomy at the root of Neoaves. *Zool. Scr.* **45**, 50–62 (2016).

15. Braun, E. L., Cracraft, J. & Houde, P. Resolving the avian Tree of Life from top to bottom: the promise and potential boundaries of the phylogenomic era. in *Avian Genomics in Ecology and Evolution: From the Lab into the Wild* (ed. Kraus, R. H. S.) 151–210 (Springer International Publishing, Cham, 2019).

16. Hackett, S. J. *et al.* A phylogenomic study of birds reveals their evolutionary history. *Science* **320**, 1763–1768 (2008).

17. Mitchell, K. J., Cooper, A. & Phillips, M. J. Comment on 'Whole-genome analyses resolve early branches in the tree of life of modern birds'. *Science* **349,** 1460 (2015).

18. Cracraft, J. *et al.* Response to Comment on 'Whole-genome analyses resolve early branches in the tree of life of modern birds'. *Science* **349**, 1460–1460 (2015).

19. Renne, P. R. *et al.* Time scales of critical events around the Cretaceous-Paleogene boundary. *Science* **339**, 684–687 (2013).

20. Hedges, S. B., Parker, P. H., Sibley, C. G. & Kumar, S. Continental breakup and the ordinal diversification of birds and mammals. *Nature* **381**, 226–229 (1996).

21. Feduccia, A. 'Big bang' for tertiary birds? *Trends in Ecology & Evolution* **18**, 172–176 (2003).

22. Mayr, G. *Paleogene Fossil Birds*. (Springer International Publishing, 2022). doi:10.1007/978-3-030-87645-6.

23. Claramunt, S. & Cracraft, J. A new time tree reveals Earth history's imprint on the evolution of modern birds. *Sci Adv* **1**, e1501005 (2015).

24. Oliveros, C. H. *et al.* Earth history and the passerine superradiation. *Proc. Natl. Acad. Sci. U. S. A.* **116**, 7916–7925 (2019).

25. McCormack, J. E. *et al.* A phylogeny of birds based on over 1,500 loci collected by target enrichment and high-throughput sequencing. *PLoS One* **8**, e54848 (2013).

26. Zwickl, D. J. & Hillis, D. M. Increased taxon sampling greatly reduces phylogenetic error. *Systematic Biology* **51**, 588–598 (2002).
27. Hedtke, S. M., Townsend, T. M. & Hillis, D. M. Resolution of phylogenetic conflict in large data sets by increased taxon sampling. *Syst. Biol.* **55**, 522–529 (2006).
28. Zhang, G. *et al.* Genomics: Bird sequencing project takes off. *Nature* **522**, 34 (2015).
29. Chen, M.-Y., Liang, D. & Zhang, P. Phylogenomic resolution of the phylogeny of laurasiatherian mammals: exploring phylogenetic signals within coding and noncoding sequences. *Genome Biol. Evol.* **9**, 1998–2012 (2017).
30. Edwards, S. V. *et al.* Implementing and testing the multispecies coalescent model: A valuable paradigm for phylogenomics. *Mol. Phylogenet. Evol.* **94**, 447–462 (2016).
31. Mirarab, S., Nakhleh, L. & Warnow, T. Multispecies coalescent: theory and applications in phylogenetics. *Annu. Rev. Ecol. Evol. Syst.* **52**, 247–268 (2021).
32. Suh, A., Smeds, L. & Ellegren, H. The dynamics of incomplete lineage sorting across the ancient adaptive radiation of neoavian birds. *PLoS Biol.* **13**, e1002224 (2015).
33. Cracraft, J. Avian higher-level relationships and classification: nonpasseriforms. *The Howard and Moore complete checklist*.
34. Mirarab, S. *et al.* A region of suppressed recombination misleads neoavian phylogenomics. *In press PNAS*.
35. Sayyari, E. & Mirarab, S. Testing for polytomies in phylogenetic species trees using quartet frequencies. *Genes* **9**, (2018).
36. Solís-Lemus, C., Yang, M. & Ané, C. Inconsistency of species tree methods under gene flow. *Syst. Biol.* **65**, 843–851 (2016).
37. Harvey, M. G. *et al.* The evolution of a tropical biodiversity hotspot. *Science* **370**, 1343–1348 (2020).
38. Moyle, R. G. *et al.* Tectonic collision and uplift of Wallacea triggered the global songbird radiation. *Nat. Commun.* **7**, 12709 (2016).
39. Cloutier, A. *et al.* Whole-genome analyses resolve the phylogeny of flightless birds (Palaeognathae) in the presence of an empirical anomaly zone. *Syst. Biol.* **68**, 937–955 (2019).

549 40. Nabhan, A. R. & Sarkar, I. N. The impact of taxon sampling on phylogenetic inference: a review
550 of two decades of controversy. *Brief. Bioinform.* **13**, 122–134 (2012).
551 41. Heath, T. A., Hedtke, S. M. & Hillis, D. M. Taxon sampling and the accuracy of phylogenetic
552 analyses. *J. Syst. Evol.* **46**, 239–257 (2008).
553 42. Lozano-Fernandez, J. A practical guide to design and assess a phylogenomic study. *Genome*
554 *Biol. Evol.* **14**, (2022).
555 43. Pick, K. S. *et al.* Improved phylogenomic taxon sampling noticeably affects nonbilaterian
556 relationships. *Mol. Biol. Evol.* **27**, 1983–1987 (2010).
557 44. Houde, P., Braun, E. L. & Zhou, L. Deep-time demographic inference suggests ecological
558 release as driver of neoavian adaptive radiation. *Diversity* **12**, 164 (2020).
559 45. Yoder, J. B. *et al.* Ecological opportunity and the origin of adaptive radiations. *J. Evol. Biol.* **23**,
560 1581–1596 (2010).
561 46. Western, D. & Ssemakula, J. Life history patterns in birds and mammals and their evolutionary
562 interpretation. *Oecologia* **54**, 281–290 (1982).
563 47. Berv, J. S. & Field, D. J. Genomic signature of an avian Lilliput effect across the K-Pg
564 extinction. *Syst. Biol.* **67**, 1–13 (2018).
565 48. Berv, J. S. *et al.* Molecular early burst associated with the diversification of birds at the K–Pg
566 boundary. *bioRxiv* 2022.10.21.513146 (2022) doi:10.1101/2022.10.21.513146.
567 49. Ksepka, D. T. *et al.* Tempo and pattern of avian brain size evolution. *Curr. Biol.* **30**, 2026–
568 2036.e3 (2020).
569 50. Sangster, G. *et al.* Phylogenetic definitions for 25 higher-level clade names of birds. *Avian*
570 *Research* **13**, 100027 (2022).
571

572

573 ## Figure Captions

574 Fig. 1: **Relationships and divergence times for 363 bird species based on 63,430 intergenic loci**. **a,**
575 Topology simplified to orders with higher clade names following [50]. Numbers on branches represent
576 local posterior probability if below 1. **b,** Timetree of all species. Gray bars are 95% credible intervals
577 for age estimates. Dots indicate nodes with fossil calibrations. Asterisks mark the three branches
578 lacking full support. A tree with tip labels is shown in Extended Data Fig. 2,3. Bird drawings by Jon
579 Fjeldså.
580

581 Fig. 2: **Explaining difficult placements. a,** Gene tree discordance across the backbone of the main tree.
582 Node colors and numbers refer to the bar plots of quartet frequencies for three possible resolutions around
583 each branch. **b,** Uncertainty at the base of Elementaves. Phaethontimorphae+Aequornithes had high local
584 posterior probability (LocalPP), but global bootstrap resampling (GlobalBS) revealed an alternative
585 placement. Violin plots (points for the species-poor Phaethontiformes) show higher root-to-tip distances of
586 Phaethontiformes and particularly Eurypygiformes than Aequornithes, which may cause attraction to the
587 long-branched Telluraves. **c,** Adding taxa occasionally impacts topology and support. Across 41,918 gene
588 trees with at least one species from each group, the alternative placement of Afroaves+Accipitriformes had
589 higher quartet support when only few species were sampled but declined with increasing taxon sampling
590 (left), particularly of Passeriformes: The main topology dominated when ≥138 passerines were sampled
591 (middle, arrow). The support for Telluraves+Elementaves decreased with increasing taxon sampling
592 (right).
593

594 Fig. 3: **Effect of increasing data quantity**. In a-c, species trees were reconstructed from subsets of gene
595 trees (1000, 2000, ..., 32,000) of the 63k intergenic regions in 50 replicates. **a,** Adding loci increases
596 similarity to the main tree (left) and increases the proportion of highly supported nodes (right). **b,** The main
597 tree with branches colored according to the difficulty of consistently recovering the clade across subsets.
598 Most branches were consistently obtained with only 1000 gene trees (gray). The remaining 40 branches
599 required more loci. **c,** Increasing the number of loci decreases the number of possible sister groups. We
600 recorded the number of unique sister groups for each node across subsets. The color corresponds to the
601 difficulty (from b), the shading and number shows the frequency with which the main topology was
602 obtained. The top row illustrates examples of easy nodes, where the same sister group was consistently
603 recovered with 2000, 4000, and 16,000 loci, respectively. The remaining plots show the most difficult
604 nodes, where multiple sister groups were supported even when 32,000 loci were subsampled. **d,** Ten
605 selected species trees, data types used in each, and the support for all challenging branches (labeled in b).
606 Asterisks indicate relationships in Passeriformes that differ from previous studies.
607

608 **Fig. 4: Phylogenetic signal across the genome**. **a,** Protein-coding regions give more varied species
609 trees when they are subsampled. Each heatmap cell shows the average Robinson-Foulds distance
610 between 1250 (diagonal: 1225) pairs of species trees each built from 2000 gene trees of different data
611 types. The values in brackets give the same metrics for 8000 gene trees, omitting UCEs which had
612 fewer loci. **b,** Effect of subsetting loci by data type and different metrics. The y-axis is the number of
613 differences to the main tree. The x-axis shows two metrics split into four quartiles from low to high.
614 Phylogenetic informativeness is the proportion of parsimony-informative sites. Clocklikeness is the
615 coefficient of variation in root-to-tip distances, a measure of misleading signals such as long branches.
616 Extended Data Fig. 8g shows other metrics. **c,** Patterns of phylogenomic incongruence along the
617 genome. Using the 94k loci binned every ~500 kb, lines show Robinson-Foulds distances to the main
618 tree (top), variance in GC content (middle), and recombination rate (bottom). Horizontal lines indicate
619 genome-wide averages.
620

621 **Fig. 5: Biological implications of the new timetree. a,** The main tree fits morphological traits well.
622 We measured phylogenetic signal (Pagel's lambda) for nine traits over 100 replicates and compared
623 the fit based on the main tree, the Prum et al.[2] topology, and the main tree with random species
624 sampling to match the sample size of Prum (one-sided t-test with Bonferroni correction). **b,** The
625 Cretaceous–Paleogene (K–Pg) and the Paleogene–Neogene transitions were associated with increased
626 effective population sizes of some lineages. Shown are the midpoint ages of each branch compared
627 with the ratio between its length in time units and in coalescent units, which is proportional to the
628 relative effective population size of that branch and generation time. Numbers correspond to selected
629 nodes from Fig. 2a. **c,** Variations in body mass and relative brain size over time changed in different
630 directions after the K–Pg event. Solid lines indicate mean values and ribbons mark 95% confidence
631 intervals. The dashed parts of the reconstruction (from 25 Ma) indicate possible uncertainty due to the
632 lack of within-family sampling (Extended Data Fig. 11g). **d,** Substitution rates increased around the
633 K–Pg boundary. Estimated molecular rates for the intergenic regions are plotted against the midpoint
634 age of each branch.
635

Methods

Further details on methods are given in the Supplementary Information.

Selection of genomic regions for phylogenomic inference

For the main tree, we used putatively intergenic regions extracted from the Cactus whole genome alignment [4,51]. We converted the HAL alignment to MAF format using chicken as the reference and extracted the best aligned synteny blocks from each query species using 10 kb windows (https://github.com/Secretloong/Cactus_Alignments_Tools, using HALtools [52] v.2.3), skipping regions that were repetitive in chicken or those only present in Galliformes. Among the first 2 kb of each window, the 1 kb portion with the most site-wise occupancy was selected to avoid portions with few sequences. The decision to use 1 kb loci from which to estimate gene trees (GTs) was made after preliminary assessments (Extended Data Fig. 1d). Therefore, loci were 8-9 kb apart, reducing the risk of strong linkage [53]. We excluded fragmentary sequences (<50% of the median length of all sequences of the locus) and loci with <4 sequences. This resulted in 94,402 loci, for which we estimated GTs. Based on the chicken genomic annotation, we identified 1 kb loci which had overlap with exons (14,355 loci) or introns (16,617 loci) and created smaller datasets without these regions (Extended Data Fig. 1b). Subtracting these from the total loci resulted in 63,430 purely intergenic loci, which were used to construct the main tree.

We also extracted loci of other data types and applied the same filtering described above. This resulted in 44,846 intronic, 14,972 exonic, and 4985 UCE loci. Introns were extracted from the Cactus alignment following previously described procedures [4] , reconstructing individual GTs for each intron of the same gene. Protein-coding regions were obtained from genome annotations [4] and all exons of the same gene were analyzed as one locus. These were further filtered and aligned. This was done with an iterative PASTA [54] v1.8.5 pipeline that included TreeShrink [55] v1.3.1 to remove outlier sequences, alignment with MAFFT [56] v7.149b G-INS-i with a variable scoring matrix [57] to isolate potentially unrelated segments, and removal of these blocks. We excluded third codon positions because they were previously shown to be problematic [1]. UCE loci were extracted using PHYLUCE [58] v1.6.3 (commit 185b705) targeting 5060 UCEs and 1000 bp flanking regions. After filtering, 5006

667 UCE loci remained. Alignment and exclusion of outliers was conducted similar to the
668 protein-coding regions but using MAFFT L-INS-i without removal of alignment segments.

669 **Generation of gene trees and species trees**

670 A total of 159,205 GTs were estimated using maximum likelihood (ML) tree inference with
671 Pargenes [59] v.1.1.0, which employs substitution model selection using Modeltest-NG [60]
672 v.0.1.3 and RAXML-NG [61] v.0.9.0 with 10 random and 10 parsimony starting trees and
673 scaled branch lengths. To identify and collapse poorly supported branches before running
674 ASTRAL, we used IQTREE [62] v.1.6.12 to perform parametric approximate likelihood ratio
675 tests (aLRT), which are fast tests of the three possible nearest-neighbor resolutions around a
676 branch [63] and are more computationally efficient than bootstrapping. Outputs from Pargenes
677 were used for computing aLRT scores. Poorly supported branches were contracted to
678 polytomies using newick-utilities [64] v.1.6 if their aLRT value was <0.95.
679
680 Collapsed GT were summarized into a coalescent-based species tree using ASTRAL-III [65]
681 v.5.14.5. Support was assessed using the posterior probability (PP). We also performed gene-
682 only multi-locus bootstrapping (globalBS) for cases where uncertainty is not local (e.g., two
683 placements many branches away both result in high quartet support), a scenario that can
684 mislead the local PP support [66]. Additionally, we tested polytomy null hypotheses [35] and
685 evaluated the quartet score of the three alternative nearest neighbor interchanges around each
686 branch [66]. Quartet scores were visualized using DiscoVista [67]. We evaluated alternative
687 species trees (e.g., moving Phaethontimorphae) by scoring these trees against the same input
688 GTs using ASTRAL.
689
690 For a concatenated analysis of the 63k loci under ML, we used RAXML-NG v.1.0.1,
691 partitioning by locus (63k partitions) with their previously determined substitution models.
692 We ran 20 independent searches from random starting trees and picked the highest-scoring
693 tree. We then ran 50 tree searches on BS pseudo-replicate alignments, judged sufficient
694 according to the MRE bootstrap convergence criterion [68]. To save time and energy, we used a
695 topological constraint for all tree searches (ML and BS). This was a strict consensus of the
696 ASTRAL trees (63k loci, exons, introns, UCEs) and of an initial ML run on the 63k loci
697 (based on 10 tree searches with 5 random+5 parsimony, no BS). This consensus left the

backbone nodes free to be inferred while constraining uncontroversial nodes within orders (317 nodes resolved, 45 collapsed).

Fossil calibration and molecular dating

We performed molecular dating using a Bayesian sequential-subtree approach [69]. This involved using date estimates from an initial analysis of a backbone tree (56 tips), containing two representatives of each of 11 subtrees. This provided secondary calibrations for subsequent dating analyses of 11 subtrees (19–42 tips each). The subtrees were then attached to the backbone to assemble a timetree of all 363 taxa.

We performed molecular dating using a subset of the 63k loci. For all loci, we estimated phylograms in IQTREE [70] v2.0.4 under GTR+F+R4, fixed to the main topology, and rooted with FastRoot [71]. We selected 10,494 loci with the lowest coefficient of variation in root-to-tip distances, thereby retaining the most clocklike loci. For locus partitioning, we randomly divided loci into two groups of 5247, within which we partitioned based on their macro-, intermediate, and microchromosomal origin. The two locus groups were used for dating. Half of the loci were used to date the backbone tree and the other half were used to date the subtrees, thus avoiding data duplication in the likelihood.

For node-based calibrations, we identified 34 clades with fossils fulfilling best practice criteria [72] (Supplementary Information). We used the CladeDate [73] method to generate calibration densities empirically based on fossil occurrences (187 fossils) and estimators of distributions in which the truncation was the estimated age of the clade [23,74] We used the Strauss and Sadler [75] estimator for uniformly distributed fossil occurrences; otherwise, we excluded the Quaternary record or used estimators that do not assume sample uniformity [73]. The resultant distributions of clade ages were used to fit Student-skew distributions to parameterize calibration priors.

The posterior distributions of the ages of the 11 nodes in the backbone tree that corresponded to the root nodes of the subtrees were fitted with *skew-t* densities using the R function sn::st.mple v.2.0.0, under the BFGS method for parameter optimisation [76]. The *skew-t* parameters were then used to specify the prior distributions of root ages for the dating analyses of the subtrees.

Bayesian molecular dating was conducted using MCMCtree [77] v.4.9h, with approximate likelihood calculation [78] and under the GTR+G model. The analyses included all calibration priors, a minimum bound on the root age based on an uncontroversial neornithine fossil [79], and a soft maximum bound at 86.5 Ma. Nodes without calibrations followed a birth-death process prior [80] ($\lambda = \mu = 1$, sampling fraction $\rho = 0.1$), which gives an approximately uniform kernel. We used a relaxed clock with lognormally distributed rates across branches and a gamma-Dirichlet prior on rates across the three subsets of loci [81]. During Markov chain Monte Carlo sampling, samples were drawn every 2500 steps over a total of 5.5×10^7 steps after 5×10^6 burn-in, run twice.

We performed four additional analyses with alternative settings (Extended Data Fig. 6): 1) Uniform calibration priors with ranges spanning the 95% probability density of the original calibration prior, adding a soft maximum bound with a 2.5% tail of probability. 2) A Jurassic age bound with a relaxed maximum age bound of 201.3 Ma on the root. 3) A calibration subset of 23 calibrations that were considered to be the most reliable. 4) A set of 10,494 loci randomly selected from the 63k set, split into two equal groups of 5247, and randomly partitioned into three subsets of 1749 loci.

Subsetting analyses

Taxon sampling. To investigate the impact of sampling multiple species across orders (which represent the most contentious branches), we successively reduced the taxon sampling to 50, 25, 10, … 2, or 1 species per order. We randomly selected species from the existing GTs of the 63k locus set, retaining all if less than the desired number were available. We then scored the main tree against the taxon-reduced GTs to compute the normalized quartet support for the three topologies around each branch. These analyses showed substantial impact only for Accipitriformes, where >50 species were required to recover the main relationship. Since only Passeriformes had >50 taxa, we inferred that their sampling impacted the position of Accipitriformes. To test this, we removed 1, 3, ... 171 of the 173 Passeriformes in a random order and computed quartet scores with GTs restricted to that subset. Two replicates produced indistinguishable results.

Data quantity. Of the 63k loci of the main analysis, we randomly selected subsets of increasing numbers of GT up to maximally half of the available GTs (1000, 2000, … 32,000). Each subset was repeated 50x and an ASTRAL tree was estimated for each. The subset topology was compared to the main tree by counting the number of differing branches (Robinson-Foulds (RF) distance/2) using TreeCmp [82] v.2.0 the proportion of highly supported branches (PP≥0.95). We recorded whether each clade of the main tree was present in subset trees, and counted how many different sister groups were present across the 50 replicates of each subset. We performed the same analyses for the other data types, maximally sampling about half of the available loci. This included exons (50x sampling 1000, 2000, … 8000 GTs), introns (1000, 2000, … 32,000), and UCEs (1000, 2000). We also performed the analyses using all non-coding (80k windows, intron, UCEs, totaling 129,878 loci) GTs (1000, 2000, … 64,000).

Data type. We compared the topological differences between trees for each data type while controlling for the number of GTs used. We subsampled loci at random (50x). The highest number of GTs subsets present across all data types was 2000 (limited by the number of UCEs). To show the impact of increasing loci, we also performed the analysis for 8000 loci, omitting comparisons with UCEs. We calculated mean pairwise RF distances between resulting species trees.

Genomic characteristics. For GTs, we calculated the number of taxa, tree length, tree diameter, stemminess, clocklikeness, mean branch support, and proportion of branches with aLRT >95 and >99. For gene alignments, we calculated locus length, total coverage, number and proportion of parsimony informative sites, and mean and standard deviation of GC content (with seqkit [83] v.2.2.0). We predicted the difficulty of phylogenetic estimation under ML using Pythia [84] v. 1.0.0, which estimates whether the alignment is likely to result in multiple, topologically highly distinct yet statistically indistinguishable topologies. We divided loci into four equal-sized quantiles based on their values for each metric (20,011 loci based on 80k loci). We then estimated an ASTRAL tree for each quantile and calculated RF distances to the main tree.

By chromosomes and chromosomal category. We built 16 species trees from GTs of the 80k set according to their chromosomal assignment in chicken, excluding small chromosomes (<1,000 GTs, chr15, chr16, upwards from chr21). We also built species trees

for each of the chromosome size categories of birds [85], i.e. macrochromosomes (49,686 GTs), intermediate chromosomes (11,592), microchromosomes (12,740), and the Z chromosome (5,672). To investigate discordance within and across chromosomes, we calculated RF distances to the main tree for each of the collapsed GTs from the 94k set, normalized to the numbers of nodes in each GT. We investigated the potential genomic co-localization with the standard deviation of GC content, because high deviations violate common model assumptions, and with recombination rates estimated for chicken [86]. We estimated mean values using the same bins as that study (~500 kb).

Phylogenetic model adequacy

We tested for excessive amounts of non-stationary base-composition using Foster's posterior predictive simulations method [87], adapted to ML using a parametric bootstrap [88]. We also tested for misleading inferences due to substitution saturation using entropy tests on parsimony-informative sites [89]. For both tests, loci were defined as having high risk of misleading inferences under scenarios where all simulations yielded inaccurate inferences.

Investigation of specific nodes

CoalHMM. CoalHMM was used to estimate ILS levels of two clades that were difficult to resolve in our main analyses, Rheiformes and Strigiformes+Accipitriformes. We filtered and split alignment blocks into 1 Mb chunks [90], on which CoalHMM was run. We tested possible placements of Rheiformes within Palaeognathae using one representative for each order (selected to be the most contiguous genome) and for all chromosomes. CoalHMM was also run for possible placements of Strigiformes and Accipitriformes, using Passeriformes as the outgroup and Bucerotiformes to represent the remaining Afroaves. The best fitting topology was chosen based on the posterior probabilities. Under an ILS model and in the absence of phenomena such as ancient hybridization, the proportion of sites supporting topologies different from the species tree should be equal.

GC content within Palaeognathae. Because we suspected that convergent GC content between Tinamiformes and Rheiformes may impact GT estimation, we defined a measure of GC similarity (ΔGC, see Supplementary Information). It should be zero under the stationary models of evolution used for phylogenetic inference. Positive values deviate from the model

uniting Tinamiformes+Rheiformes and negative values have the reverse effect. For 54,651 of the 63k loci that had all relevant species present, we calculated ΔGC, and created nine subsets of loci. We ran ASTRAL on each subset, and all of them united Tinamiformes+Rheiformes. We computed a normalized quartet score around the branch to investigate whether subsets without high ΔGC had lower quartet support for Tinamiformes+Rheiformes.

Inference of effective population size

We compared the timetree with the coalescent unit (CU) lengths estimated by ASTRAL. For each internal branch, we computed the ratio of the branch length in time units to the CU length:

$$\frac{time\ unit}{coalescent\ unit} = \frac{generation\ time \times number\ of\ generations}{number\ of\ generations/2N_e} = 2\ generation\ time \times N_e\ .$$

Higher values are indicative of higher population size (N_e) or longer generation time. Ignoring changes to generation time, higher time/CU ratios can be attributed to larger N_e. Around the K-Pg-boundary, the generation times are presumed to have decreased, which makes the increases in our measured quantity indicative of even larger N_e growth than what would be inferred if generation times are assumed constant. Note that summary methods such as ASTRAL are known to underestimate CU length in the presence of high GT estimation error. However, we only compare branches to each other, without claiming to estimate the true N_e. Thus, as long as estimation error is not particularly concentrated on specific nodes, it should not impact the relative values.

Analysis of molecular evolutionary rates

Genome-wide evolutionary rates were estimated for each branch using the 63k loci. To minimize the estimation bias in substitution rates arising from discordance between the species tree and GTs [91], we only considered GT branches that were concordant with the main tree [92]. Each concordant branch length was divided by the time duration of the branch from the main timetree analysis, leading to a rate estimate for each species-tree branch for each locus.

Analysis of phylogenetic signal

Pagel's lambda λ [93] was measured for nine continuous morphological traits from AVONET [94]

on the main tree, the Prum et al. [2] topology, and the main tree randomly subsampled to the sample size of Prum (n=198). We also performed a comparison between trees pruned to the 124 families present in both studies. In order to account for the high proportion of Passeriformes in our study, we also excluded all but one passerine from both trees. We calculated λ for each trait using 100 simulations using phylolm [95]. To investigate potential effects of an incorrect tree topology, we simulated traits on the main tree under a Brownian motion (BM) model using fastBM [96] with λ=0.96. We then randomly changed the position of 1%, 5%, 10%, and 20% of taxa to represent incorrect relationships, repeated each 100x, and estimated λ. To investigate the effect of convergent evolution, we randomly selected species pairs consisting of one passeriform and one non-passeriform, representing 1%, 5%, 10%, and 20% of taxa. We gave each species pair the same trait value, repeated 100x, and estimated λ.

Analysis of body mass and brain size evolution

We obtained body mass data (log-transformed) for 363 species [94,97] and estimated brain size (volume of the brain case) for 228 species based on endocast volume, or back-calculated it using brain volume = brain mass/1.036 [98]. We used the average of males and females or mean unsexed values when available. For the brain size, we used missForest [99] to impute missing values based on phylogenetic relationships. Relative brain size was calculated as the residual from a log-log phylogenetic Generalized Least Square regression of absolute brain size against body mass. Ancestral states of both traits were reconstructed by Evomap using a multiple variance BM approach [100]. The variations were summarized by dividing the phylogeny into bins of 1 Ma and averaging in each over all branches.

The rates of evolution in both traits were analyzed using BayesTraits [101] v.4 with variable rates models and default priors. Each analysis ran for 110 million iterations with a burn-in of 10 million in triplicates. We used the convergence diagnostic test of coda [102] and selected the run with the highest mean marginal likelihood. We also compared the fit of three single-process models (BM, early burst (EB), Ornstein–Uhlenbeck (OU)) using Geiger [103] v.2. To compare model fit using AIC (Extended Data Fig. 11e), we used the mean of the rate-scaled trees of BayesTraits and calculated the likelihood of a BM model on this tree with the same trait data [104]. To investigate whether sampling one species per family could impact ancestral reconstructions, we modified tip values to reflect the family's range in body size [94] across 100 replicates (Extended Data Fig. 11f). We also confirmed that inclusion of the imputed brain size values did not change the shape of ancestral reconstructions (Extended Data Fig. 11g).

Data availability

The genome assemblies analyzed in this study and their whole genome alignment were part of the study by Feng et al. [4] and accession numbers are given as part of the Supplementary Data. Alignments, gene trees and species trees, in addition to data files produced for their analysis and scripts to plot the figures are available at https://doi.org/10.17894/ucph.85624f66-c8e5-4b89-8e8a-fe984ca89e4a [105]. This repository also contains a file detailing contents and commands to use for individual and batch download of files. The study analyzed morphological trait data from AVONET [94] (https://figshare.com/s/b990722d72a26b5bfead) and from https://doi.org/10.5061/dryad.fbg79cnw7 [97], recombination rates for chicken [86] (https://static-content.springer.com/esm/art%3A10.1186%2F1471-2156-11-11/MediaObjects/12863_2009_758_MOESM5_ESM.XLS), and time-calibrated species trees from Jarvis et al. [1] (http://gigadb.org/dataset/101041) and Prum et al. [2] (Avian-TimeTree.tre from https://zenodo.org/records/28343).

Code availability

Code used for producing the figures in this manuscript is available at https://doi.org/10.17894/ucph.85624f66-c8e5-4b89-8e8a-fe984ca89e4a [105]. The pipeline to extract synteny blocks from the whole genome alignment is available under https://github.com/Secretloong/Cactus_Alignments_Tools. The pipeline to filter and align loci is available under https://github.com/uym2/TreeShrink/tree/master/related_scripts.

References (Methods)

51.Armstrong, J. *et al.* Progressive Cactus is a multiple-genome aligner for the thousand-genome era. *Nature* **587**, 246–251 (2020).

52.Hickey, G., Paten, B., Earl, D., Zerbino, D. & Haussler, D. HAL: a hierarchical format for storing and analyzing multiple genome alignments. *Bioinformatics* **29**, 1341–1342 (2013).

53.Springer, M. S. & Gatesy, J. Delimiting coalescence genes (C-genes) in phylogenomic data sets. *Genes* **9**, (2018).

54.Mirarab, S. *et al.* PASTA: ultra-large multiple sequence alignment for nucleotide and amino-acid sequences. *J. Comput. Biol.* **22**, 377–386 (2015).

55.Mai, U. & Mirarab, S. TreeShrink: fast and accurate detection of outlier long branches in collections of phylogenetic trees. *BMC Genomics* **19**, 272 (2018).

56.Katoh, K., Misawa, K., Kuma, K.-I. & Miyata, T. MAFFT: a novel method for rapid multiple sequence alignment based on fast Fourier transform. *Nucleic Acids Res.* **30**, 3059–3066 (2002).

57.Katoh, K. & Standley, D. M. A simple method to control over-alignment in the MAFFT multiple sequence alignment program. *Bioinformatics* **32**, 1933–1942 (2016).

58.Faircloth, B. C. PHYLUCE is a software package for the analysis of conserved genomic loci. *Bioinformatics* **32**, 786–788 (2016).

59.Morel, B., Kozlov, A. M. & Stamatakis, A. ParGenes: a tool for massively parallel model selection and phylogenetic tree inference on thousands of genes. *Bioinformatics* **35**, 1771–1773 (2019).

60.Darriba, D. *et al.* ModelTest-NG: a new and scalable tool for the selection of DNA and protein evolutionary models. *Mol. Biol. Evol.* **37**, 291–294 (2020).

61.Kozlov, A. M., Darriba, D., Flouri, T., Morel, B. & Stamatakis, A. RAxML-NG: a fast, scalable and user-friendly tool for maximum likelihood phylogenetic inference. *Bioinformatics* **35**, 4453–4455 (2019).

62.Nguyen, L.-T., Schmidt, H. A., von Haeseler, A. & Minh, B. Q. IQ-TREE: a fast and effective stochastic algorithm for estimating maximum-likelihood phylogenies. *Mol. Biol. Evol.* **32**, 268–274 (2015).

63.Anisimova, M. & Gascuel, O. Approximate likelihood-ratio test for branches: A fast, accurate, and powerful alternative. *Syst. Biol.* **55**, 539–552 (2006).

64.Junier, T. & Zdobnov, E. M. The Newick utilities: high-throughput phylogenetic tree processing in the UNIX shell. *Bioinformatics* **26**, 1669–1670 (2010).

65.Zhang, C., Sayyari, E. & Mirarab, S. ASTRAL-III: increased scalability and impacts of contracting low support branches. in *Comparative Genomics. RECOMB-CG 2017. Lecture Notes in Computer Science* (eds. Meidanis, J. & Nakhleh, L.) 53–75 (Springer International Publishing,

945 2017).
946 66.Sayyari, E. & Mirarab, S. Fast coalescent-based computation of local branch support from
947 quartet frequencies. *Mol. Biol. Evol.* **33**, 1654–1668 (2016).
948 67.Sayyari, E., Whitfield, J. B. & Mirarab, S. DiscoVista: interpretable visualizations of gene
949 tree discordance. *Mol. Phylogenet. Evol.* **122**, 110–115 (2018).
950 68.Pattengale, N. D., Alipour, M., Bininda-Emonds, O. R. P., Moret, B. M. E. & Stamatakis, A.
951 How many bootstrap replicates are necessary? *J. Comput. Biol.* **17**, 337–354 (2010).
952 69.Álvarez-Carretero, S. *et al.* A species-level timeline of mammal evolution integrating
953 phylogenomic data. *Nature* **602**, 263–267 (2022).
954 70.Minh, B. Q. *et al.* IQ-TREE 2: new models and efficient methods for phylogenetic inference
955 in the genomic era. *Mol. Biol. Evol.* **37**, 1530–1534 (2020).
956 71.Mai, U., Sayyari, E. & Mirarab, S. Minimum variance rooting of phylogenetic trees and
957 implications for species tree reconstruction. *PLoS One* **12**, e0182238 (2017).
958 72.Parham, J. F. *et al.* Best practices for justifying fossil calibrations. *Syst. Biol.* **61**, 346–359
959 (2012).
960 73.Claramunt, S. CladeDate: calibration information generator for divergence time estimation.
961 *Methods Ecol. Evol.* **13**, 2331–2338 (2022).
962 74.Marshall, C. R. Using the fossil record to evaluate timetree timescales. *Front. Genet.* **10**, 1049
963 (2019).
964 75.Strauss, D. & Sadler, P. M. Classical confidence intervals and Bayesian probability estimates
965 for ends of local taxon ranges. *Math. Geol.* **21**, 411–427 (1989).
966 76.Azzalini, A. A. *The R Package Sn: The Skew-Normal and Related Distributions such as the*
967 *Skew-T and the SUN (version 2.1.1)*. (Università degli Studi di Padova, Italia, 2019).
968 77.Yang, Z. PAML 4: phylogenetic analysis by maximum likelihood. *Mol. Biol. Evol.* **24**, 1586–
969 1591 (2007).
970 78.Thorne, J. L., Kishino, H. & Painter, I. S. Estimating the rate of evolution of the rate of
971 molecular evolution. *Mol. Biol. Evol.* **15**, 1647–1657 (1998).
972 79.Slack, K. E. *et al.* Early penguin fossils, plus mitochondrial genomes, calibrate avian

evolution. *Mol. Biol. Evol.* **23**, 1144–1155 (2006).

80.Yang, Z. & Rannala, B. Bayesian estimation of species divergence times under a molecular clock using multiple fossil calibrations with soft bounds. *Mol. Biol. Evol.* **23**, 212–226 (2006).

81.Dos Reis, M., Zhu, T. & Yang, Z. The impact of the rate prior on Bayesian estimation of divergence times with multiple loci. *Syst. Biol.* **63**, 555–565 (2014).

82.Bogdanowicz, D., Giaro, K. & Wróbel, B. TreeCmp: comparison of trees in polynomial time. *Evol. Bioinform. Online* **8**, EBO.S9657 (2012).

83.Shen, W., Le, S., Li, Y. & Hu, F. SeqKit: a cross-platform and ultrafast toolkit for FASTA/Q file manipulation. *PLoS One* **11**, e0163962 (2016).

84.Haag, J., Höhler, D., Bettisworth, B. & Stamatakis, A. From easy to hopeless-predicting the difficulty of phylogenetic analyses. *Mol. Biol. Evol.* **39**, (2022).

85.International Chicken Genome Sequencing Consortium. Sequence and comparative analysis of the chicken genome provide unique perspectives on vertebrate evolution. *Nature* **432**, 695–716 (2004).

86.Elferink, M. G., van As, P., Veenendaal, T., Crooijmans, R. P. M. A. & Groenen, M. A. M. Regional differences in recombination hotspots between two chicken populations. *BMC Genet.* **11**, 11 (2010).

87.Foster, P. G. Modeling compositional heterogeneity. *Syst. Biol.* **53**, 485–495 (2004).

88.Duchêne, D. A., Duchêne, S. & Ho, S. Y. W. New statistical criteria detect phylogenetic bias caused by compositional heterogeneity. *Mol. Biol. Evol.* **34**, 1529–1534 (2017).

89.Duchêne, D. A., Mather, N., Van Der Wal, C. & Ho, S. Y. W. Excluding loci with substitution saturation improves inferences from phylogenomic data. *Syst. Biol.* **71**, 676–689 (2022).

90.Rivas-González, I. *et al.* Pervasive incomplete lineage sorting illuminates speciation and selection in primates. *Science* **380**, eabn4409 (2023).

91.Mendes, F. K. & Hahn, M. W. Gene tree discordance causes apparent substitution rate variation. *Syst. Biol.* **65**, 711–721 (2016).

92.Walker, J. F., Smith, S. A., Hodel, R. G. J. & Moyroud, E. Concordance-based approaches for

1001 the inference of relationships and molecular rates with phylogenomic data sets. *Syst. Biol.* **71**,
1002 943–958 (2022).
1003 93.Pagel, M. Inferring the historical patterns of biological evolution. *Nature* **401**, 877–884
1004 (1999).
1005 94.Tobias, J. A. *et al.* AVONET: morphological, ecological and geographical data for all birds.
1006 *Ecol. Lett.* **25**, 581–597 (2022).
1007 95.Ho, L. si T. & Ané, C. A linear-time algorithm for Gaussian and non-Gaussian trait evolution
1008 models. *Syst. Biol.* **63**, 397–408 (2014).
1009 96.Revell, L. J. phytools: an R package for phylogenetic comparative biology (and other things).
1010 *Methods Ecol. Evol.* **3**, 217–223 (2012).
1011 97.Székely, T. *et al.* Sex roles in birds: influence of climate, life histories and social
1012 environment. Dryad https://doi.org/10.5061/dryad.fbg79cnw7 (2022).
1013 98.Iwaniuk, A. N. & Nelson, J. E. Can endocranial volume be used as an estimate of brain size in
1014 birds? *Can. J. Zool.* **80**, 16–23 (2002).
1015 99.Stekhoven, D. J. & Bühlmann, P. MissForest--non-parametric missing value imputation for
1016 mixed-type data. *Bioinformatics* **28**, 112–118 (2012).
1017 100. Smaers, J. B., Mongle, C. S. & Kandler, A. A multiple variance Brownian motion
1018 framework for estimating variable rates and inferring ancestral states. *Biol. J. Linn. Soc. Lond.*
1019 **118**, 78–94 (2016).
1020 101. Pagel, M., Meade, A. & Barker, D. Bayesian estimation of ancestral character states
1021 on phylogenies. *Syst. Biol.* **53**, 673–684 (2004).
1022 102. Plummer, M., Best, N., Cowles, K., Vines, K. & Others. CODA: convergence
1023 diagnosis and output analysis for MCMC. *R news* **6**, 7–11 (2006).
1024 103. Pennell, M. W. *et al.* geiger v2.0: an expanded suite of methods for fitting
1025 macroevolutionary models to phylogenetic trees. *Bioinformatics* **30**, 2216–2218 (2014).
1026 104. Cooney, C. R. *et al.* Mega-evolutionary dynamics of the adaptive radiation of birds.
1027 *Nature* **542**, 344–347 (2017).
1028 105. Stiller, J., Mirarab, S. & Zhang, G. Data repository for ‘Complexity of avian

evolution revealed by family-level genomes'. https://doi.org/10.17894/ucph.85624f66-c8e5-4b89-8e8a-fe984ca89e4a.

Acknowledgements

Foremost we express gratitude to the individuals and institutions worldwide who have collected and preserved the tissue resources used to generate the genomic sequence data analyzed here [4]. This dataset includes samples obtained from 66 institutions and 56 countries, spanning the years 1982–2015. Sample contributors were either authors of the original family-phase data release [4] or acknowledged in that study according to their choosing and were invited to contribute to the development of this manuscript. We are grateful for computing resources made available through GenomeDK and to the Science Faculty at the University of Copenhagen for access to Computerome 2.0. We furthermore acknowledge the Gauss Centre for Supercomputing e. V. for funding computing time on the GCS Supercomputer SuperMUC at the Leibniz Supercomputing Centre (LRZ). Computations were also performed on the San Diego Supercomputer Center (SDSC) through the Extreme Science and Engineering Discovery Environment (XSEDE) supported by the US National Science Foundation grant number ACI-1548562 as well as high performance computational resources provided by Louisiana State University (http://www.hpc.lsu.edu). This work was supported by the New Cornerstone Science Foundation through the XPLORER PRIZE and other grants to G.Z. from Kunpeng Fellowship at Zhejiang Province, the Strategic Priority Research Program of the Chinese Academy of Sciences (XDB31020000), Villum Investigator grant (no. 25900), and International Partnership Program of Chinese Academy of Sciences (no.152453KYSB20170002). S.F. was funded by the National Natural Science Foundation of China grant (no. 32170626). D.A.D. was supported by a European Commission Marie Sklodowska-Curie Action (H2020-MSCA-IF-2019-883832). E.D.J. contributions were supported by the Howard Hughes Medical Institute. A.K., B.M., J.H., and A.S. were financially supported by the Klaus Tschira Foundation, by DFG grant STA 860/6-2, and by the European Union (EU) under Grant Agreement No 101087081 (Comp-Biodiv-GR). S.C. is supported by the Natural Sciences and Engineering Research Council of Canada (NSERC) Discovery Grant RGPIN-2018-06747. P.A.H. and C.R. were supported by research grant no. 25925 from VILLUM FONDEN. J.M.T.N. is supported by an Australian Research Council Discovery Early Career Researcher Award (DE200101222). S.Y.W.H. was

supported by the Australian Research Council (FT160100167). The US National Science Foundation funded B.C.F. (DEB-1655624) and E.L.B. (DEB-1655683). T.S. was funded by The Royal Society (Wolfson Merit Award WM170050, APEX APX\R1\191045), by the National Research, Development and Innovation Office of Hungary (ÉLVONAL KKP-126949, K-116310), and by the Eötvös Loránd Research Network, ELKH – Debrecen University Reproductive Strategies Research Group (Ref 1102207). This work was facilitated by a workshop supported by a Carlsberg Foundation grant (CF19-0810) to J.S.

Author Contribution

G.Z., J.S., and S.M. conceived and designed the study. J.S., S.F., A.-A.C., I.R.-G., D.A.D., Q.F., Y.D., A.K., A.S., S.Y.W.H., B.C.F. J.H., P.A.H., M.B., U.M., G.C., R.G., C.Z., Y.X., Z.H., Z.C., Z.Y., H.A.O., L.N., B.M., R.R.d.F., M.S., A.A., E.L.B., and S.M. performed genomic analyses and phylogenetic analyses. S.C., J.M.T.N., P.H., J.C., B.L. and J.F.. developed fossil-based temporal calibrations. J.A.T., T.S., J.D.K., A.L. and C.R. contributed to trait data collection. J.S., S.F., A.-A.C., I.R.-G., D.A.D, A.K., A.S., S.C., J.M.T.N., S.Y.W.H., B.C.F, P.H., J.C., J.F., P.A.H., R.R.d.F., B.P., J.A.T., T.S., A.H.R., A.L., M.S., A.A., D.T.T., M.B., G.R.G., M.H.S., T.W., E.L.B., M.T.P.G., E.D.J., S.M., G.Z. contributed to the data interpretation. F.L., C.R., G.R.G., M.T.P.G., E.D.J., and G.Z. initiated the B10K project. J.F. contributed the bird drawings used in the figures. J.S., S.M., and G.Z. wrote the manuscript with input from all co-authors.

Competing Interest

M.T.P.G. serves on the Science Advisory Board of Colossal Laboratories & Biosciences. All other authors declare no competing interests.

Additional Information

Supplementary Information is available for this paper. Correspondence and requests for materials should be addressed to Josefin Stiller (josefin.stiller@bio.ku.dk), Siavash Mirarab (smirarabbaygi@ucsd.edu), and Guojie Zhang (guojiezhang@zju.edu.cn). Reprints and permissions information is available at www.nature.com/reprints.

Extended Data Captions

Extended Data Fig. 1 Overview of the phylogenomic dataset. a, Overview of the datasets by different data types in terms of number of loci and base pairs analyzed. **b,** Comparison of dataset size to previous studies focused on avian relationships. **c,** Schematic overview of the extraction of different genomic data types (intergenic regions, exons, UCEs, introns). **d,** Choice of the length of intergenic loci. To evaluate the impact of locus length of intergenic regions, we used 500 alignments of 10 kb length and extracted subregions of increasing length (0.25 kb to 5 kb) to build gene trees for each. We then calculated the number of well-supported nodes of each locus compared to the next shorter version of the locus. We found that gene tree support increased up to 1 kb length indicating that phylogenetic signal increased. At lengths greater than 1 kb an increasing number of gene trees had fewer well-supported nodes than at shorter locus lengths (values below 0 in the plot), perhaps due to increasing propensity to include recombinations in a locus. We therefore chose 1 kb as the locus length for our analyses to balance high signal and reduced chance of recombination.

Extended Data Fig. 2 The main dated tree with tip labels for all groups except Passeriformes. Taxonomic orders are annotated to the right of the tree. Colors of the branches follow those used in Fig. 1. The Passeriformes portion of the tree is shown in Extended Data Fig. 3.

Extended Data Fig. 3 The main dated tree with tip labels for Passeriformes. Taxonomic family names are given on the branches. Major clades as discussed in the text are annotated to the right following [24].

Extended Data Fig. 4 Overview of topologies for the species trees obtained for different data types. Each tree is simplified to taxonomic orders, colors follow those used in Fig. 1. All analyses are coalescent-based species trees obtained from ASTRAL with support being local posterior probabilities, with the exception of the values on the panel showing the topology obtained from concatenated analysis using RAxML-NG with support values resulting from bootstrapping. Poorly supported branches (bootstrap < 0.8, local posterior probabilities < 0.9) are dashed.

Extended Data Fig. 5 Comparison of the main tree with previous studies simplified to taxonomic orders. Top, comparison to Jarvis et al. 2014 [1] 'TENT' on the right. Bottom, comparison with Prum et al. 2015 [2] on the right. Bands connect the same tips, dashed branches on the right tree indicate nodes not present in the main tree.

Extended Data Fig. 6 Comparison of inferred ages to previous studies and across alternative analyses. a, Age estimates in comparison to previous studies for major clades and orders (left) and for families (right). Shown are median age estimates (points) and 95% credible intervals (whiskers) derived from MCMC sampling for clades that were present in at least two studies. The dashed line is the K–Pg boundary. **b-e,** Comparison of age estimates between the main analysis and alternative analyses. Red arrows indicate the amount of displacement in the date estimates from the main analysis compared with each alternative analysis. For a description of each analysis, refer to the Methods.

Extended Data Fig. 7 Exploration of difficult nodes. a, Removing species one by one from Columbea and Otidimorphae (rows, heatmap) changed the support for Columbea in the gene trees as measured by the difference between the quartet score of the tree placing Columbea or Mirandornithes at the base. Columbea was not recovered unless all but one Columbiformes or Cuculiformes was removed. Large differences between mean (blue; n=63,430; shown with s.e.m.) and median (green) show the impact of outlier genes: While the mean score (akin to what is used by ASTRAL) favored Columbea in some cases, the median never favored it. **b,** Genome-wide scan for the competing topologies for Phaethontimorphae. The main (blue) and the alternative (brown) topology had a normalized quartet score difference of 0.000537%. Chromosomes with <100 windows were excluded. The y-axis shows the quartet support for a bipartition in each gene tree minus the mean support for that topology across all gene trees, calculated as a moving average over 100 loci. If a genomic region was strongly in favor of either topology, the two lines would be diverging, but this was not observed. **c,** The two competing positions (colors as in b) for Phaethontimorphae were responsive to selecting subsets of the intergenic regions that targeted long branches (panels with gray background). Species trees were generated from gene trees split into four quartiles according to their values for seven metrics. For each resulting species tree, the position of Phaethontimorphae is shown (PP=1 throughout). **d,** Comparison of root-to-tip distances across 21,154,875 gene tree tips as an indicator of susceptibility to long-branch attraction. The violin plots show distributions grouped by orders as well as mean (dots) and three quartiles (horizontal lines). **e,** Comparison of GC content outliers across birds. For each species grouped by orders, the number of loci that were outliers (defined using the interquartile range) in their GC standard deviation from the remaining taxa is shown. The outliers were counted across 159k loci from all data types. Rheiformes and Tinamiformes had many loci with a different GC content compared to the remaining birds, which may artificially attract these two taxa. **f,** Effect of taxon sampling on topology. We sampled 1–10 taxa for each order and investigated the effect on specific nodes, given as the most recent common ancestor (MRCA) of two taxa. Colors indicate the number of replicates that recovered the clade. Most clades were supported irrespective of the number of taxa sampled (yellow), while Columbaves (Mesitornithiformes, Cuculiformes) was only found across all replicates when at least 3 taxa were sampled per order. The MRCA of Phaethontiformes+Strisores was only found when at least 10 taxa were sampled. Strigiformes and Accipitriformes were only recovered as a clade when more than 10 taxa were sampled (discussed in the main text). **g,** GC-content similarities between Tinamiformes and Rheiformes cause topological changes in gene trees. Positive values of the relative GC similarity indicate that Tinamiformes and Rheiformes are similar to each other but not to Apterygiformes and Casuariiformes, and negative values indicate the opposite. Using this quantity, we divided loci into bins and calculated the quartet score for each bin.

Extended Data Fig. 8 Comparisons between different data types. Colors are the same for each data type across all panels. In panels a-c, 50 subsets were drawn and summarized into species trees for each data type and each subset of n loci. Boxplot components are the same as in c. **a,** Greater dataset size resulted in increased similarity to the main tree across all data types. **b,** Greater dataset size resulted in an increased proportion of highly supported nodes of the resulting species tree across all data types. **c,** Response to increasing dataset size in comparison to different reference species trees. Each panel compares the same subsets of the 63k dataset to the reference trees (obtained from summarizing all loci of a data type), showing that increasing gene tree sampling consistently improved similarity. The increase in similarity to the species tree from concatenation and from analyzing exons is less pronounced, indicating more sustained differences despite large numbers of loci. **d-f,** Density distribution of phylogenetic signal measured as **d,** the percentage of branches in each gene tree with more than 95% support, **e,** the number of parsimony informative sites (PIS) in a locus, **f,** the predicted difficulty of each alignment using Pythia. Exons have the lowest signal and are more difficult. UCEs are longer than intergenic regions and thus have more PIS and slightly higher support on average, while the predicted difficulty of estimating trees for both is similar. Introns are heterogenous, ranging from easy to difficult. **g,** For each data type, loci were sorted according to their magnitude in seven metrics and split into four quantiles. The gene trees of each quantile were

summarized into a species tree and compared to the main tree. Exons generally responded the strongest to subsetting, while effects were less pronounced but present in the other data types.

Extended Data Fig. 9 The number of potential sister groups decreases with increasing number of loci. Only those nodes that still had multiple sister group proposals at 8k loci are shown. Points show the number of different sister group proposals obtained across 50 subsets of n loci. Shading of the nodes and orange numbers indicate the proportion with which the main topology was obtained.

Extended Data Fig. 10 Comparison of different chromosomes and chromosomal categories. a, Discordance across chromosomes. Mean ± s.e.m. of percent normalized Robinson-Foulds (RF) distance for gene trees from the 80k locus set derived from individual chromosomes (circles, left y-axis) and absolute RF distance to species trees (diamonds, right y-axis). Dashed line: mean gene tree distance across all chromosomes. Chromosomes with less than 1000 gene trees were not used to construct species trees. **b,** Mean ± s.e.m of the GC standard deviation of gene trees from the 80k locus set for each chromosome, showing a general increase in GC standard deviation in shorter chromosomes. Dashed line: mean across all chromosomes. **c,** Density plot for distribution of GC standard deviation for alignments, showing higher deviation for microchromosomes. **d,** Pearson correlation of mean normalized RF distance and recombination rate for loci of different chromosome types binned over 500 kb. No adjustments for multiple comparisons were made.

Extended Data Fig. 11 Trait evolution. a, Simulations on inferred Pagel's lambda (λ) values. To simulate topological error (left), continuous traits were simulated and an increasing proportion of species were randomly misplaced in the phylogeny (n=100). To simulate the effect of convergence in trait values (right), continuous traits were simulated on a phylogeny and an increasing proportion of species pairs were randomly given the same trait value to simulate the action of convergence (n=100). Compared to the effects of topological inaccuracies, the influence of convergently similar trait values on λ estimates was weaker. **b,** Reconstruction of rate changes in body mass evolution (log-transformed). Branches are colored by estimates of the mean rate (log-transformed); rate changes can occur in both directions, either an increase or a decrease. **c,** Reconstruction of rate changes in relative brain size evolution (residual). Branch colors as in a. Taxa with pronounced rate changes as mentioned in the main text are annotated. **d,** Model comparisons between variable-rate and single-process models (BM: Brownian motion, EB: early burst, OU: Ornstein–Uhlenbeck) for body size. **e,** Model comparisons as in d for relative brain size. **f,** Impact of taxon sampling on ancestral reconstruction of body size. The solid purple line is the result of the ancestral reconstruction of the full dataset. The gray lines are ancestral reconstructions from analyses in which each species' trait values were randomly drawn from the range of values across their family (n=100). The chosen values did not impact the reconstructions at deep timescales but estimates diverged more from 25 million years ago to the present, indicating that increased taxon sampling within families may lead to a different trajectory in more recent times. **g,** Impact of imputation on ancestral reconstructions of relative brain size. The non-imputed dataset contained only values based on the literature, while the imputed dataset included some values inferred using phylogenetic information. Solid lines indicate mean values and ribbons mark 95% confidence intervals. The two ancestral reconstructions are almost indistinguishable.

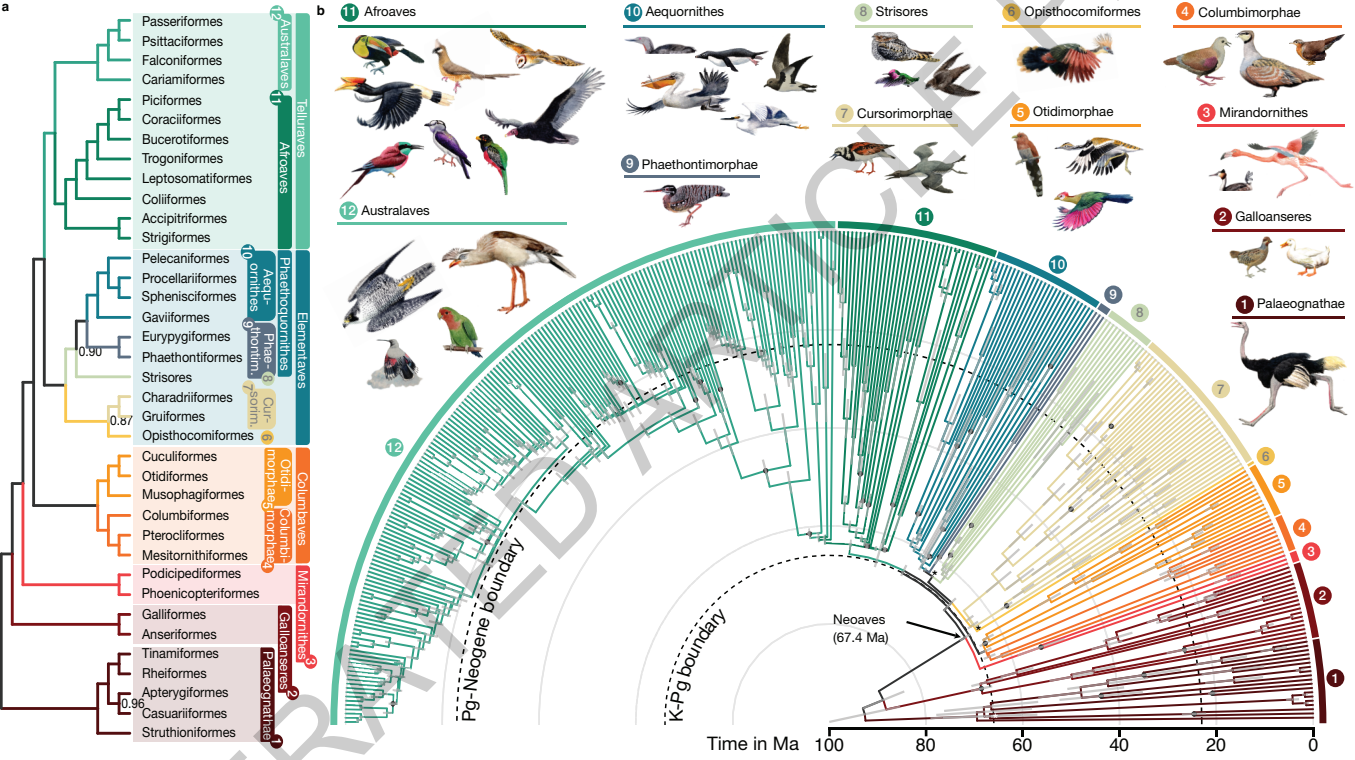
a
b
Passeriformes
Psittaciformes
Falconiformes
Cariamiformes
Piciformes
Coraciiformes
Bucerotiformes
Trogoniformes
Leptosomatiformes
Coliiformes
Accipitriformes
Strigiformes
Pelecaniformes
Procellariiformes
Sphenisciformes
Gaviiformes
Eurypygiformes
Phaethontiformes
Strisores
Charadriiformes
Gruiformes
Opisthocomiformes
Cuculiformes
Otidiformes
Musophagiformes
Columbiformes
Pterocliformes
Mesitornithiformes
Podicipediformes
Phoenicopteriformes
Galliformes
Anseriformes
Tinamiformes
Rheiformes
Apterygiformes
Casuariiformes
Struthioniformes
Australaves
Afroaves
Telluraves
Aequornithes
Phaethoquornithes
Phaethontimorphae
Cursorimorphae
Elementaves
Otidimorphae
Columbimorphae
Columbea
Mirandornithes
Galloanseres
Palaeognathae
0.90
0.87
0.96
11 Afroaves
10 Aequornithes
8 Strisores
6 Opisthocomiformes
4 Columbimorphae
7 Cursorimorphae
5 Otidimorphae
3 Mirandornithes
9 Phaethontimorphae
12 Australaves
2 Galloanseres
1 Palaeognathae
Pg-Neogene boundary
K-Pg boundary
Neoaves
(67.4 Ma)
Time in Ma
100
80
60
40
20
0

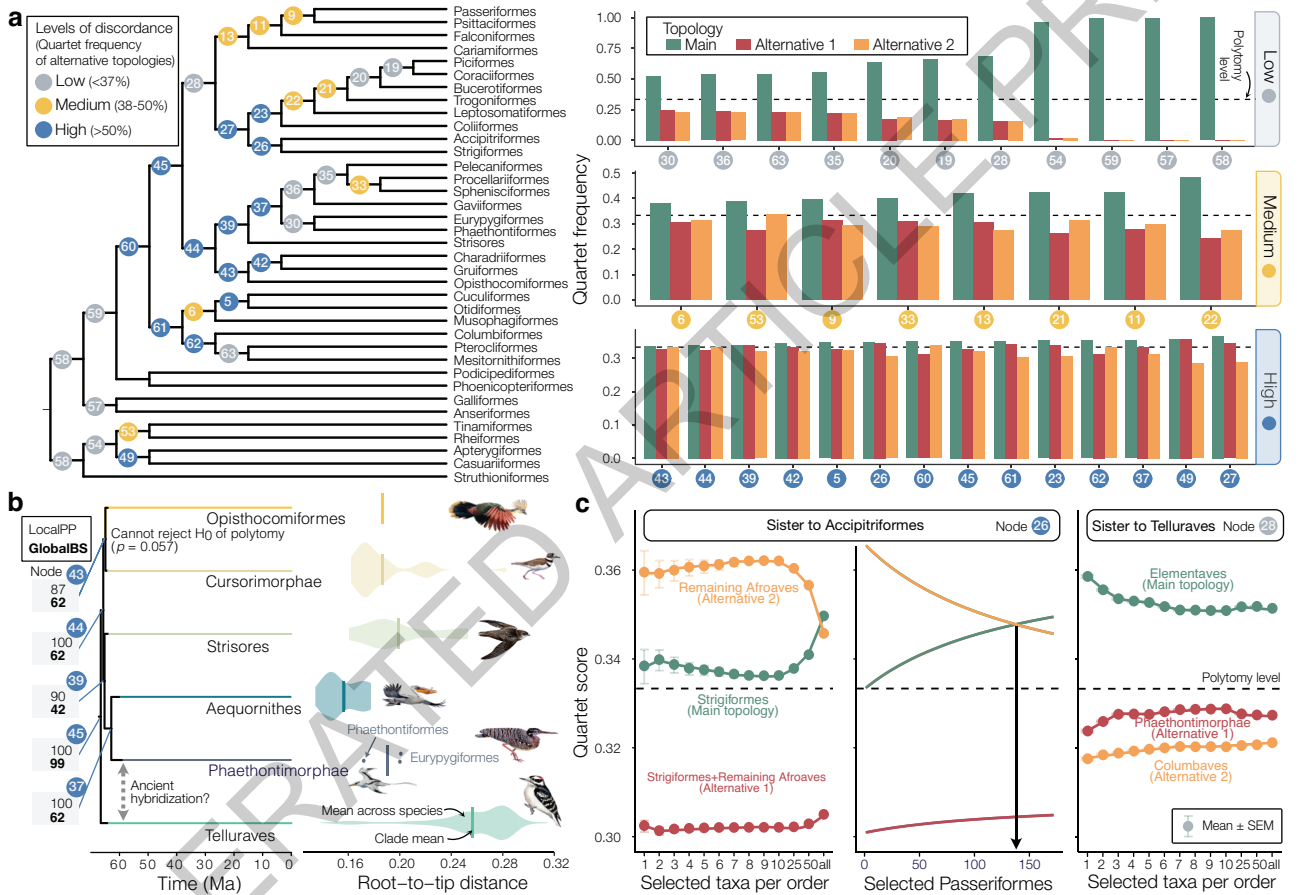

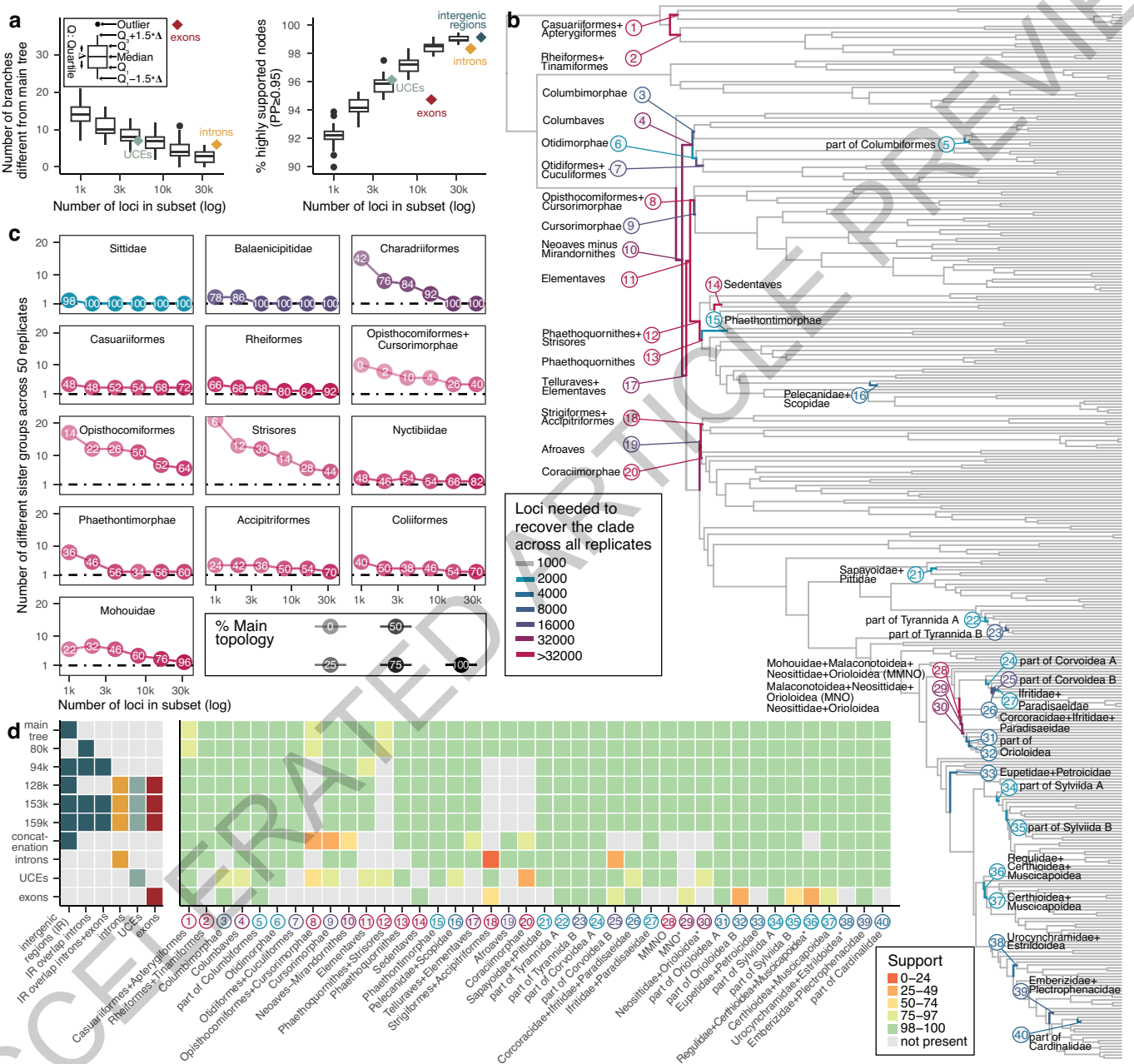

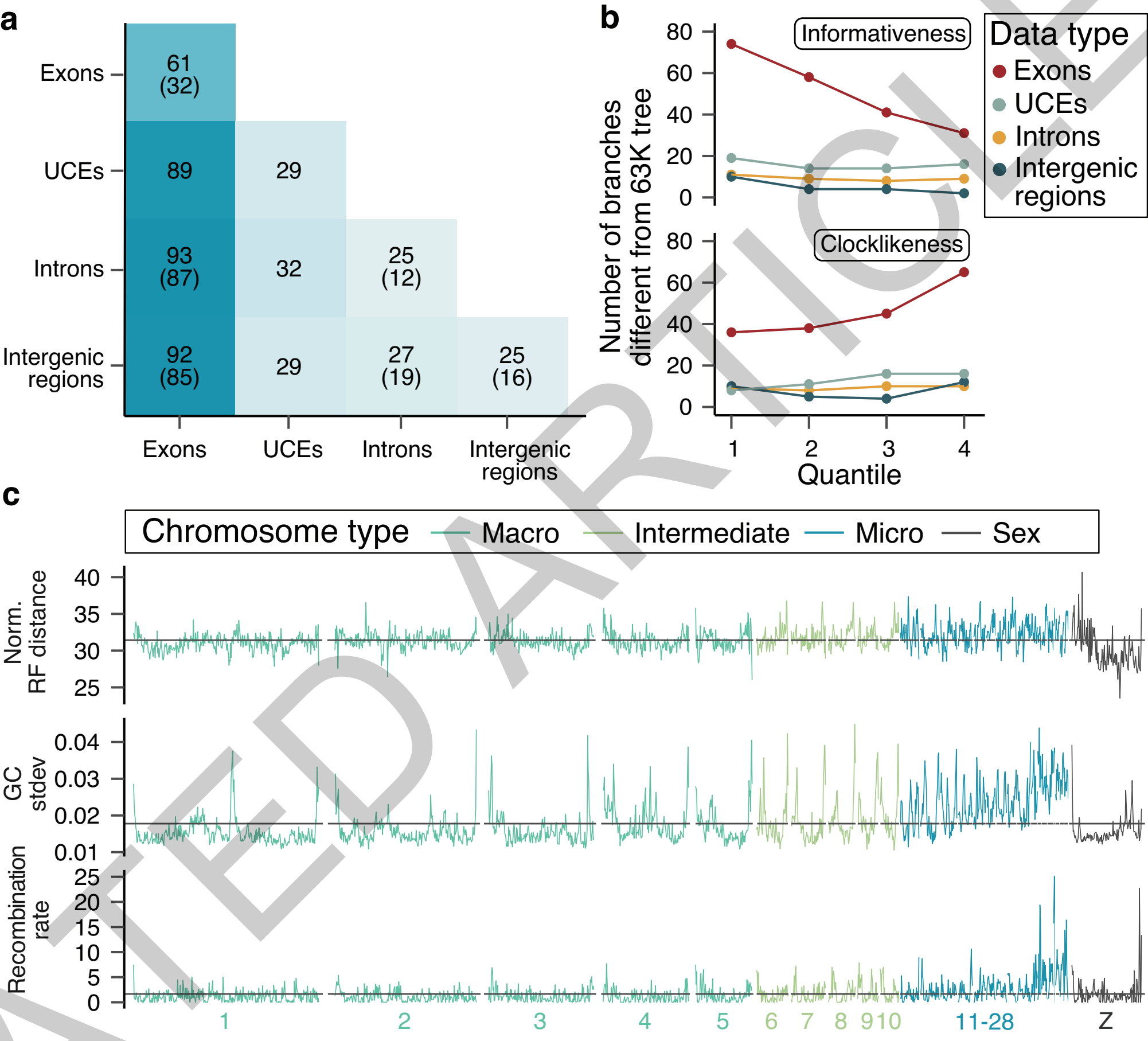

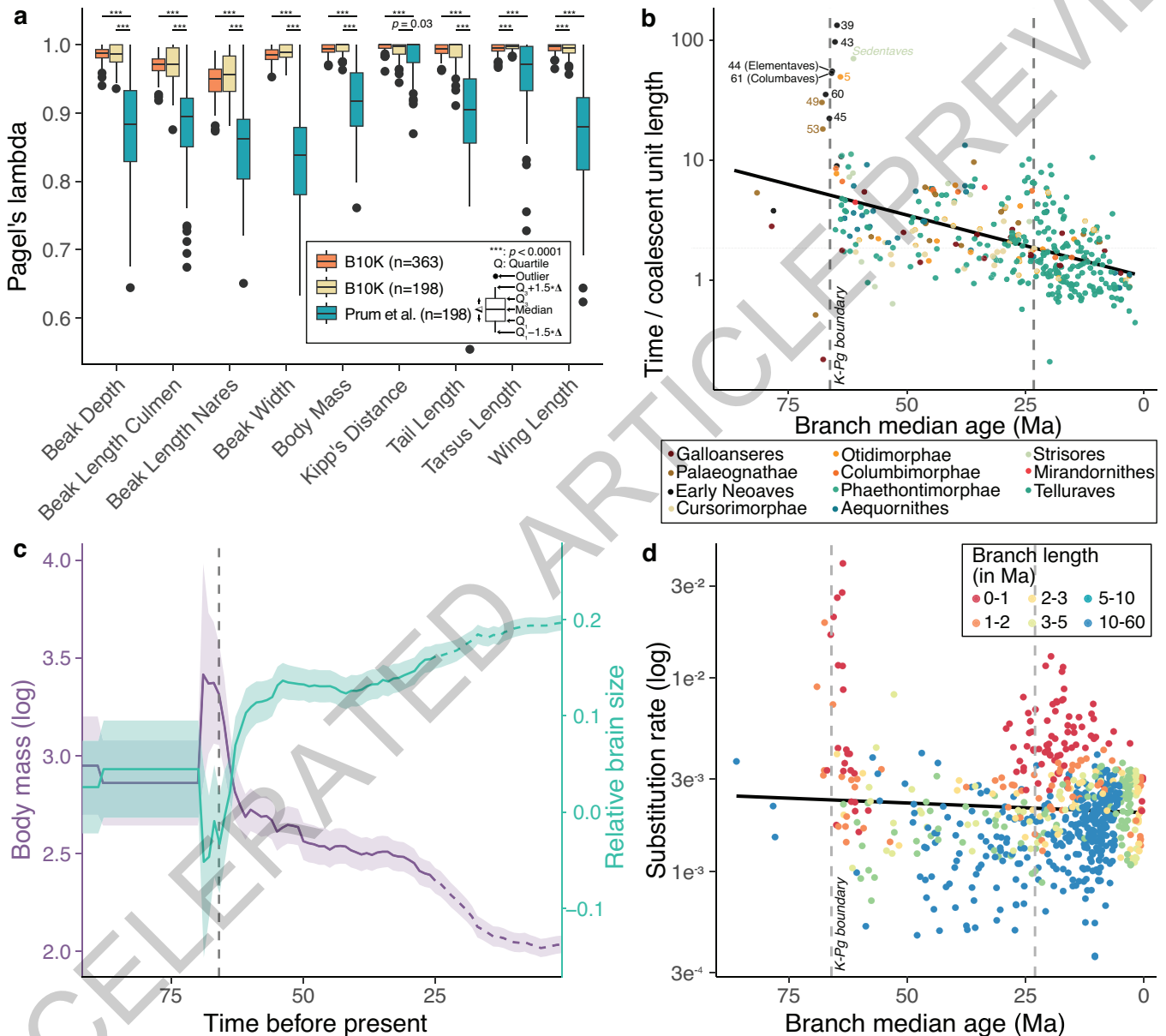

a

Dataset	Data type	Description	Loci	Base pairs
94K	Intergenic regions	All intergenic loci	94,402	94,402,000
80K	Intergenic regions	Excluding overlap with exons	80,047	80,047,000
63K	Intergenic regions	Excluding overlap with exons or introns	63,430	63,430,000
Intron	Introns	All intronic loci	44,846	136,940,000
UCE	UCEs	All Ultraconserved Element (UCE) loci	4,985	25,579,810
Exon	Exons	All exonic loci	14,972	18,975,346
128K	Total Evidence	All 63K intergenic loci + introns + UCEs + exons	128,233	244,925,156
159K	Total Evidence	All 94K intergenic loci + introns + UCEs + exons	159,205	275,897,156

b

Study	Species	Loci	Base pairs	Size of alignment	Species trees
Hackett et al. 2008, Science	169	19	0.03 Mb	5,070,000	1
Jarvis et al. 2014, Science	48	14,446	41.8 Mb	2,006,400,000	35
Prum et al. 2015, Nature	198	259	0.4 Mb	79,200,000	12
Kuhl et al. 2021, MBE	429	5,127	2.7 Mb	1,158,300,000	13
This study	363	159,205	276 Mb	99,825,000,000	1435
Increase from Jarvis	7x	10x	6x	50x	41x

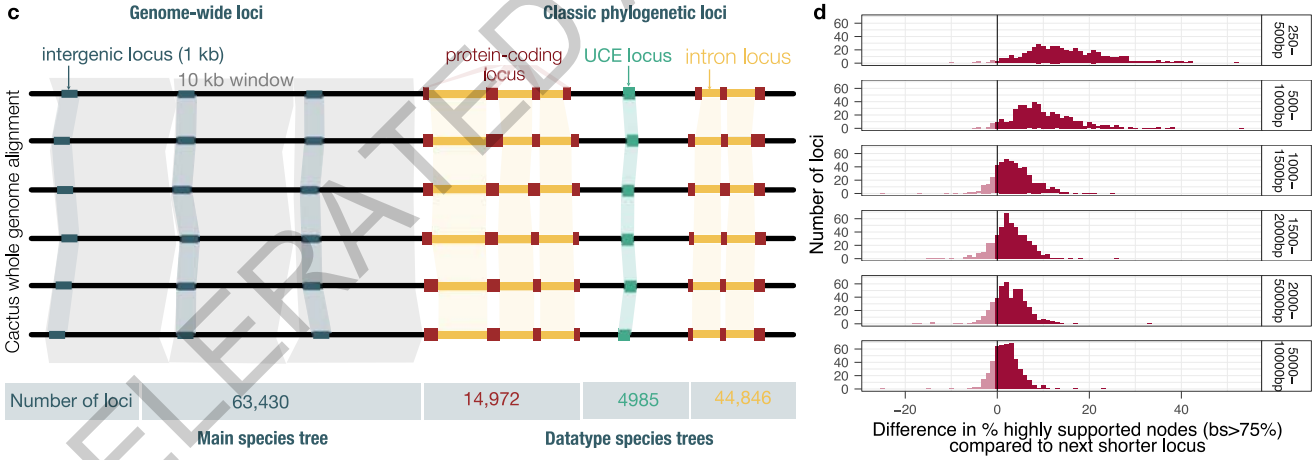

Extended Data Fig. 1

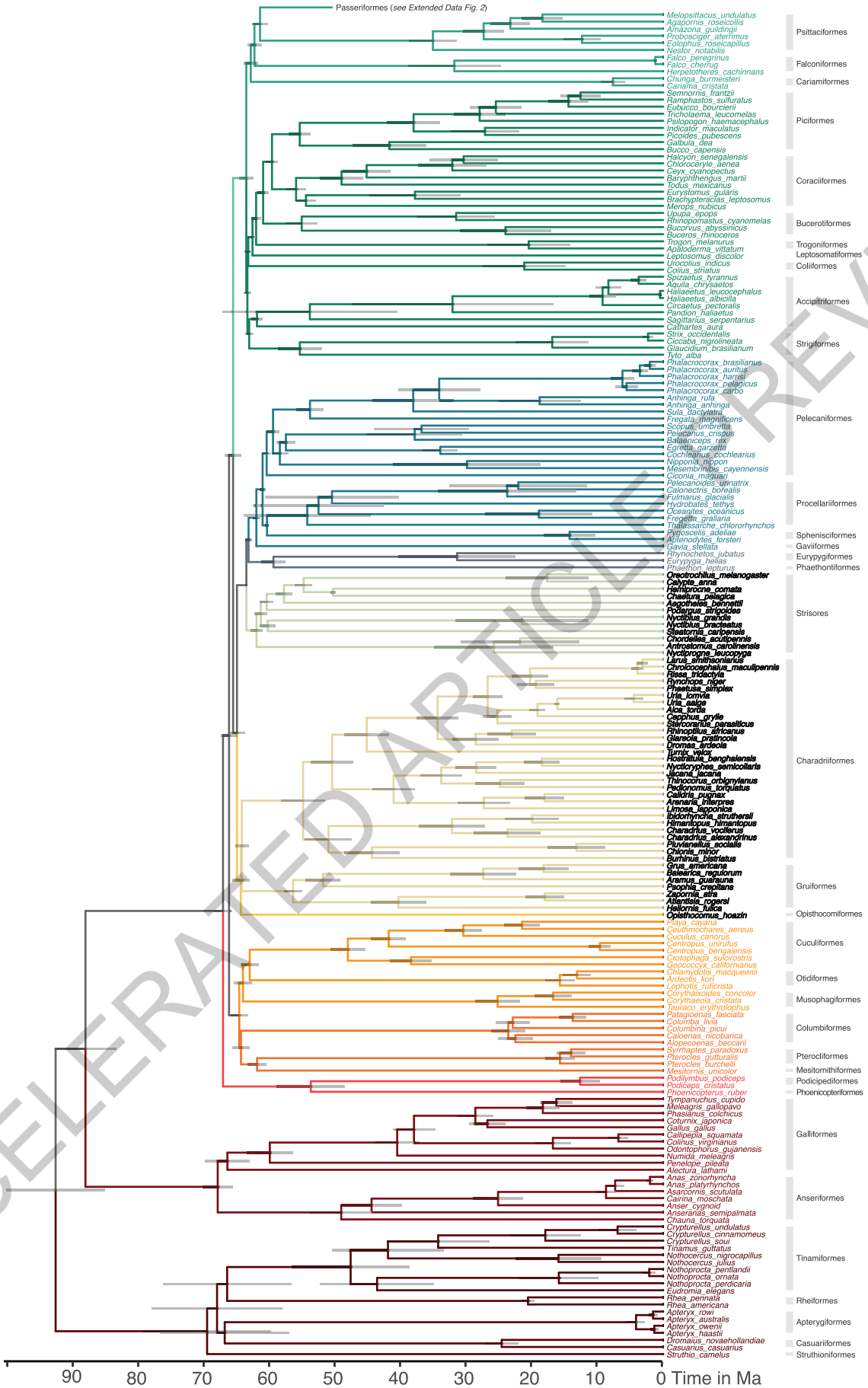

Extended Data Fig. 2

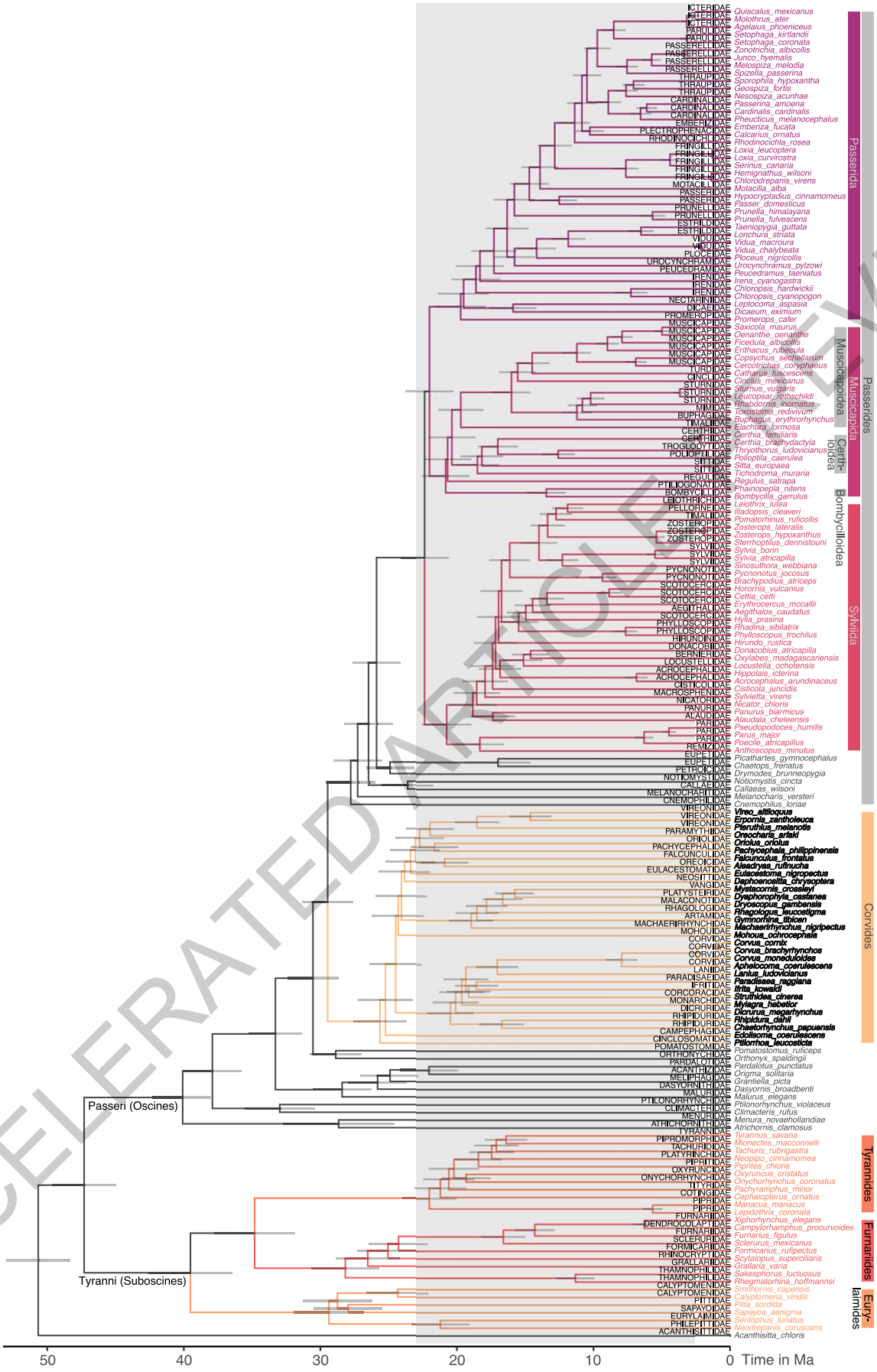

Extended Data Fig. 3

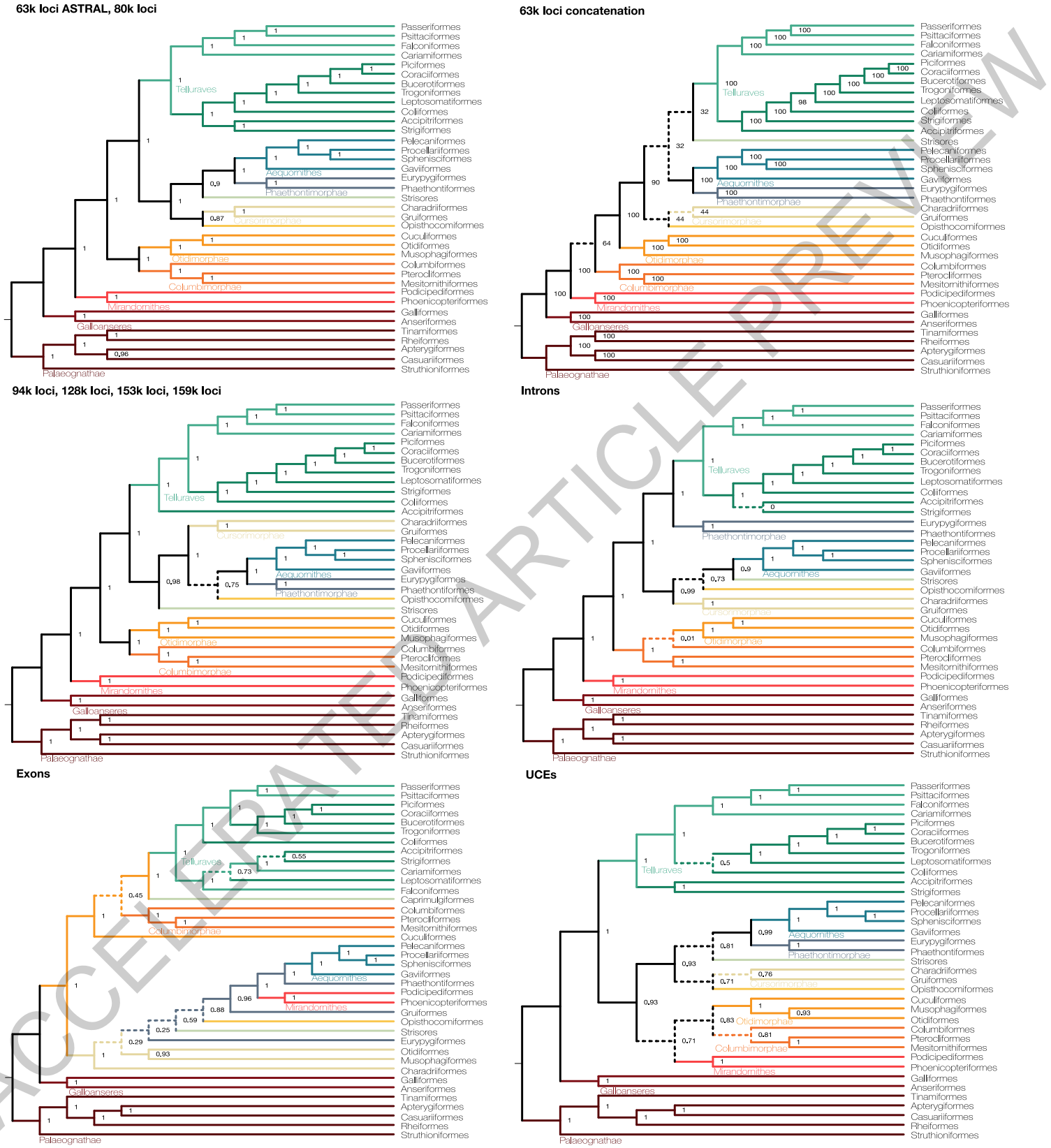

Extended Data Fig. 4

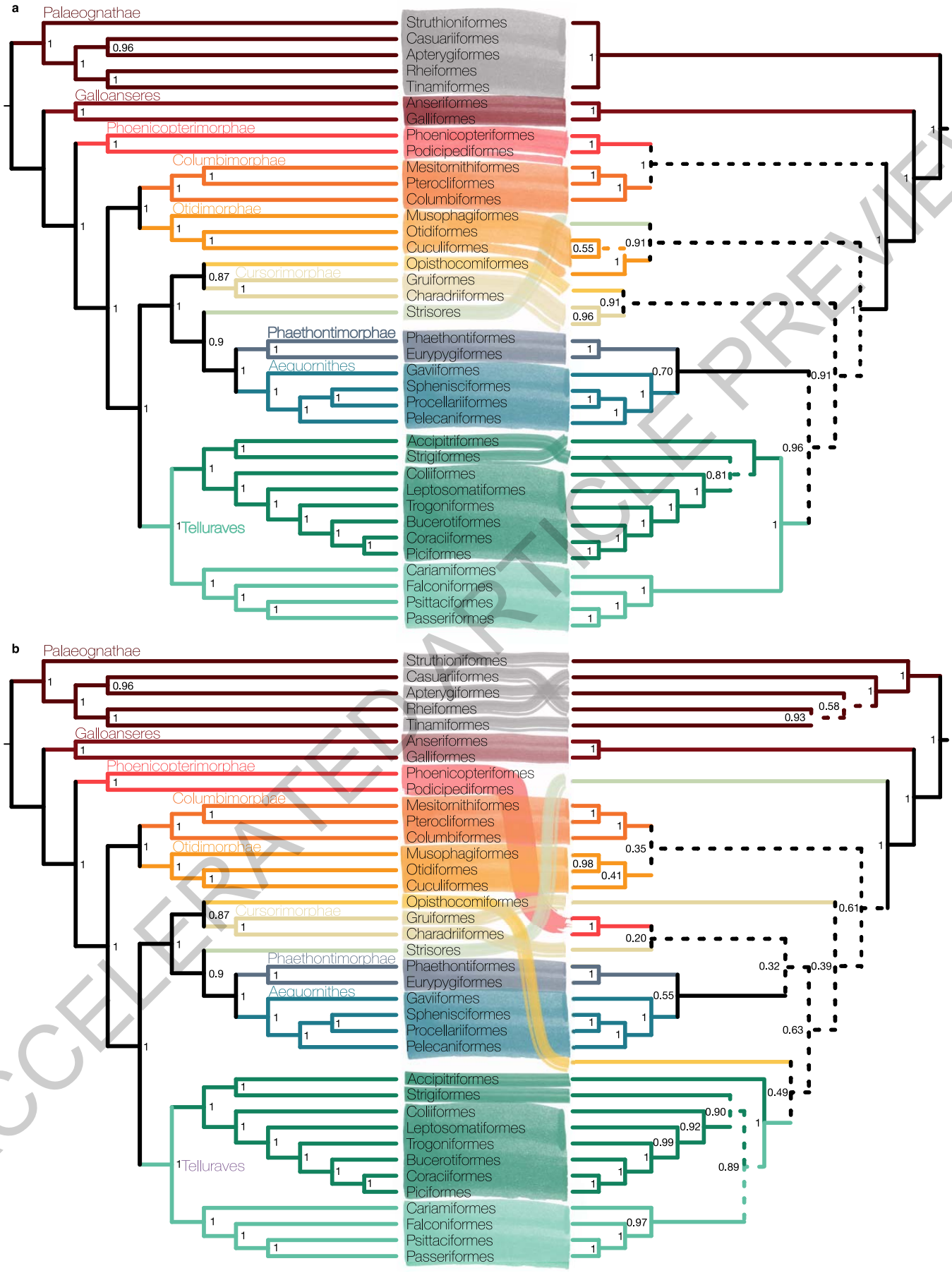

Extended Data Fig. 5

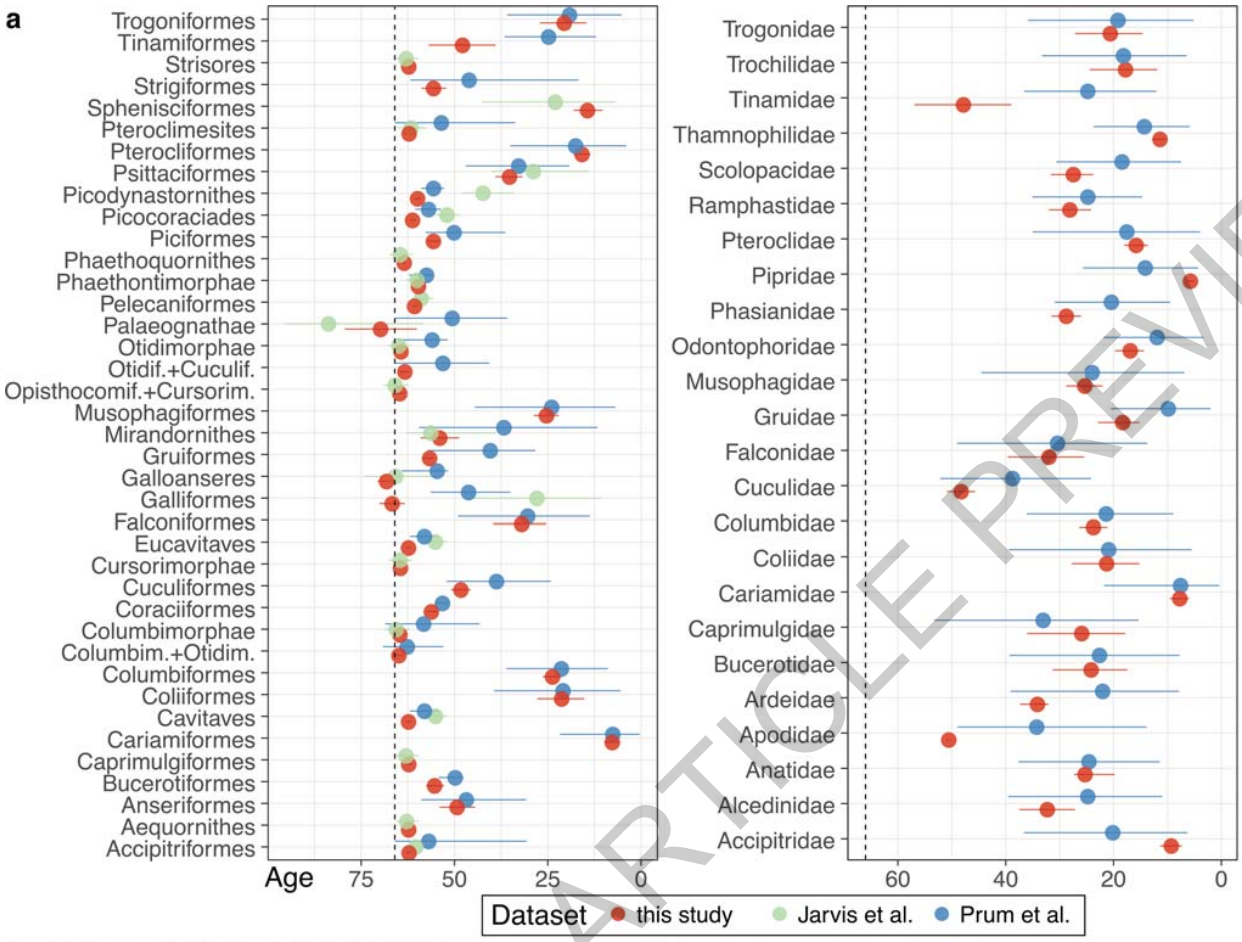

Extended Data Fig. 6

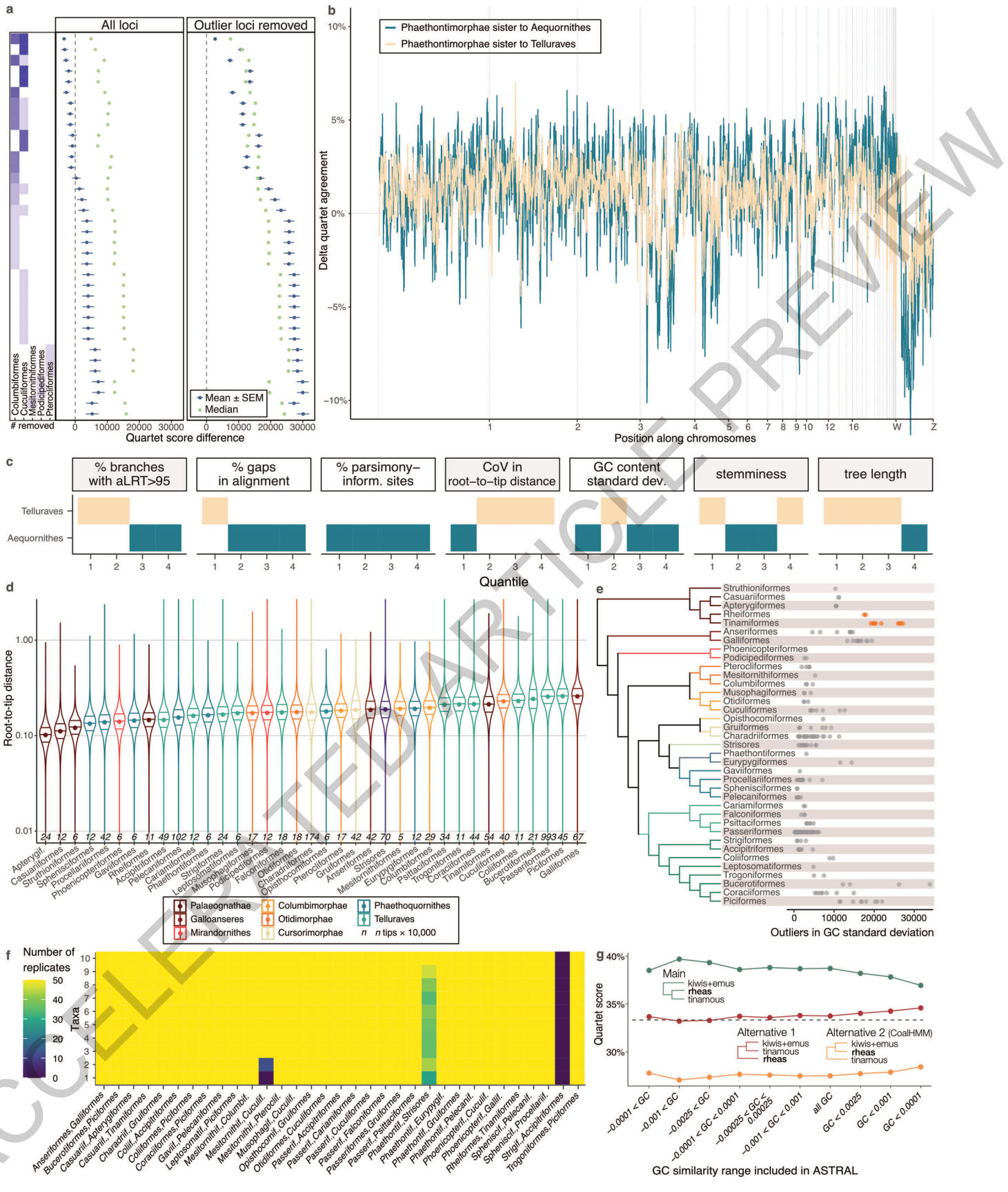

Extended Data Fig. 7

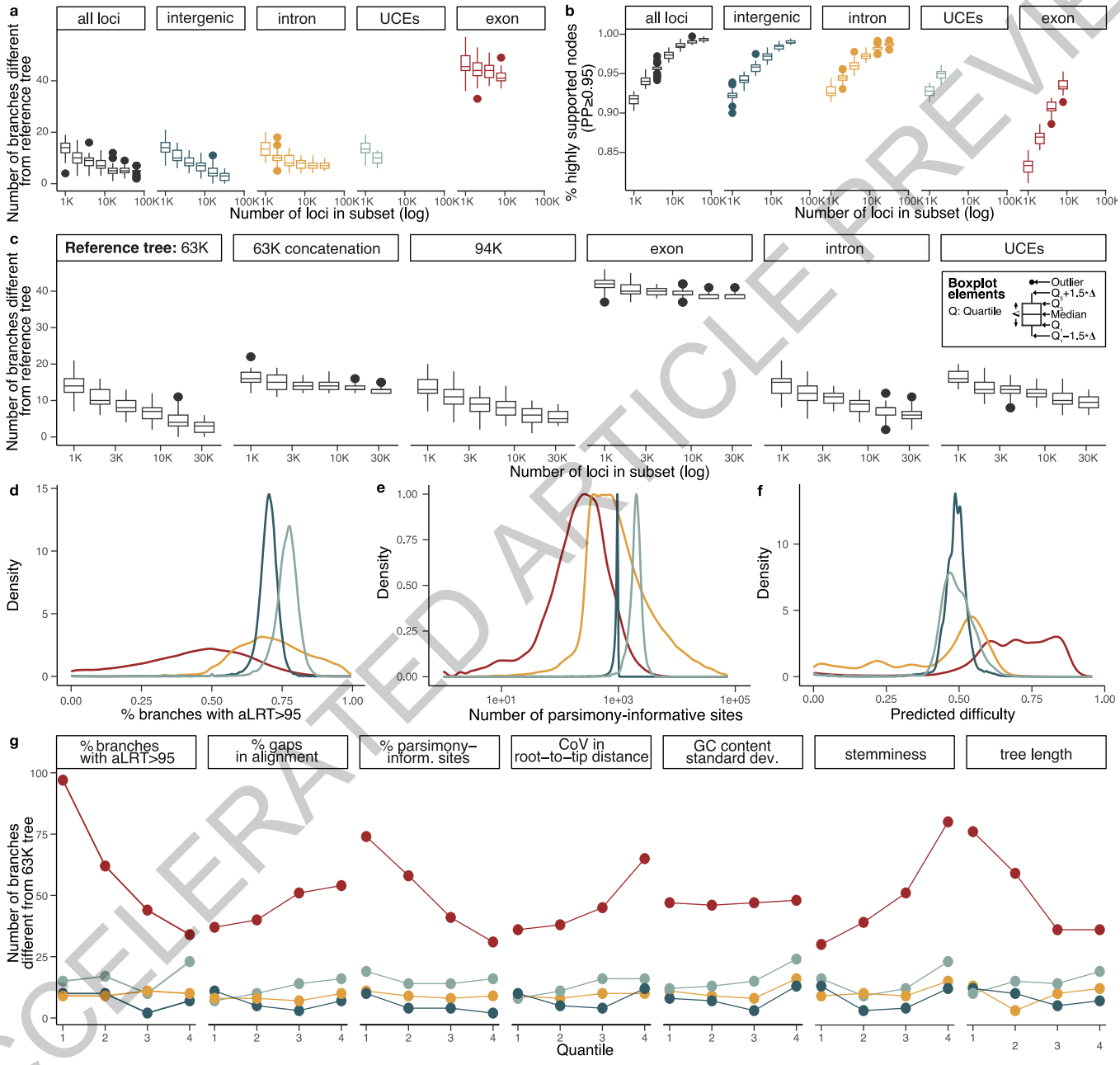

Extended Data Fig. 8

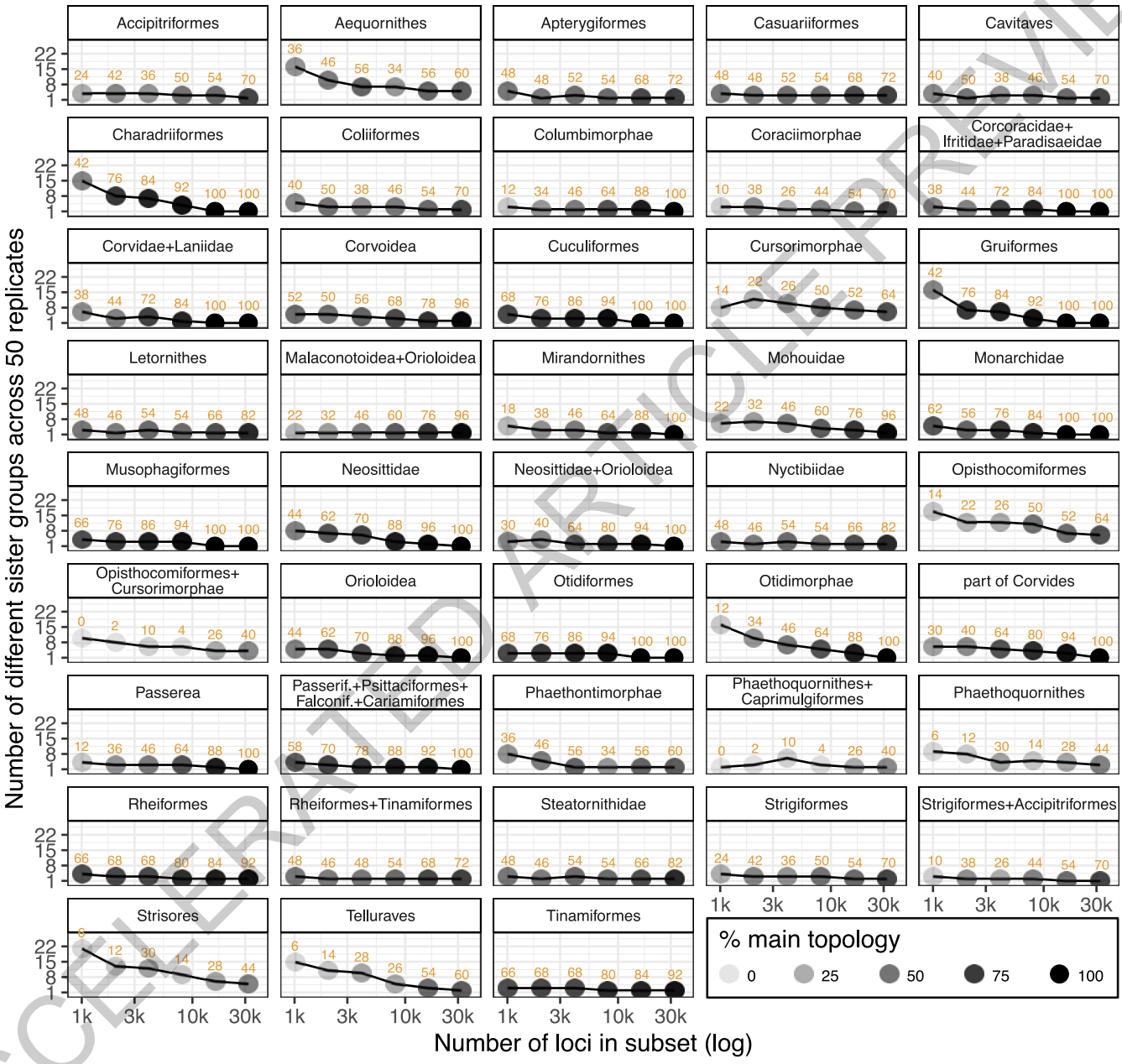

Extended Data Fig. 9

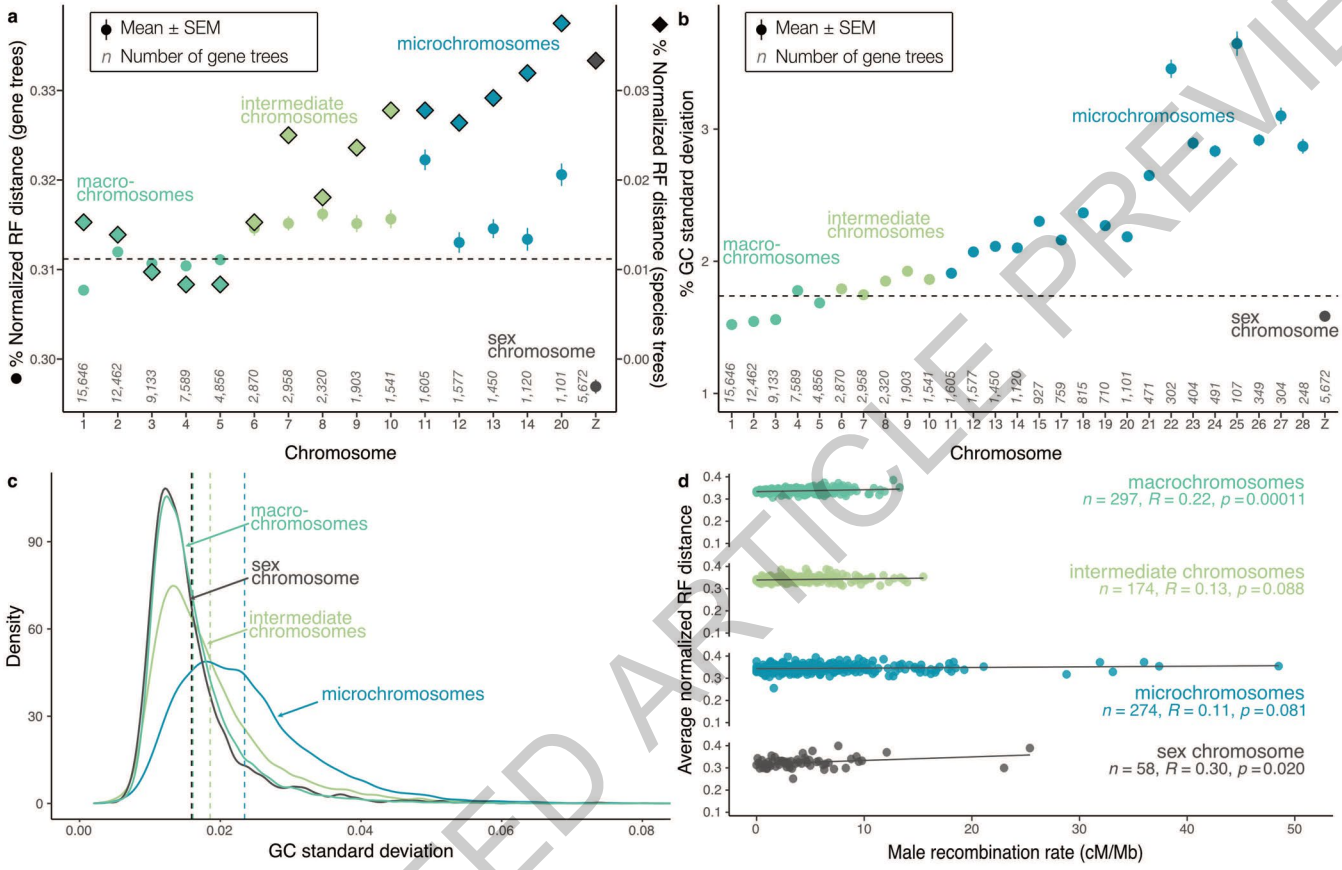

Extended Data Fig. 10

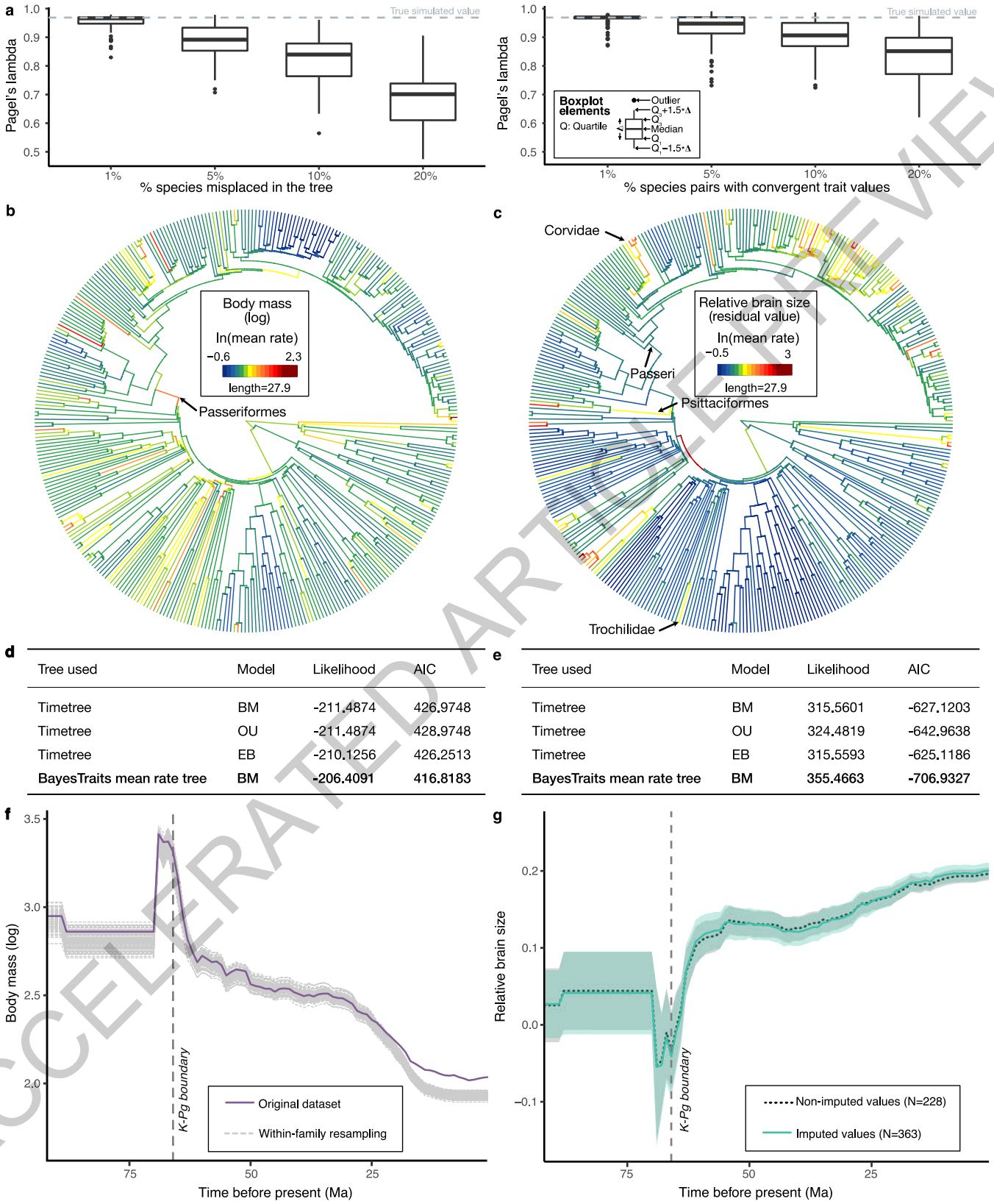

d

Tree used	Model	Likelihood	AIC
Timetree	BM	-211.4874	426.9748
Timetree	OU	-211.4874	428.9748
Timetree	EB	-210.1256	426.2513
BayesTraits mean rate tree	**BM**	**-206.4091**	**416.8183**

e

Tree used	Model	Likelihood	AIC
Timetree	BM	315.5601	-627.1203
Timetree	OU	324.4819	-642.9638
Timetree	EB	315.5593	-625.1186
BayesTraits mean rate tree	**BM**	**355.4663**	**-706.9327**

Extended Data Fig. 11

nature portfolio

Corresponding author(s): Stiller, Mirarab, Zhang

Last updated by author(s): Mar 6, 2024

Reporting Summary

Nature Portfolio wishes to improve the reproducibility of the work that we publish. This form provides structure for consistency and transparency in reporting. For further information on Nature Portfolio policies, see our Editorial Policies and the Editorial Policy Checklist.

Statistics

For all statistical analyses, confirm that the following items are present in the figure legend, table legend, main text, or Methods section.

n/a	Confirmed	
☐	☒	The exact sample size (*n*) for each experimental group/condition, given as a discrete number and unit of measurement
☐	☒	A statement on whether measurements were taken from distinct samples or whether the same sample was measured repeatedly
☐	☒	The statistical test(s) used AND whether they are one- or two-sided *Only common tests should be described solely by name; describe more complex techniques in the Methods section.*
☒	☐	A description of all covariates tested
☐	☒	A description of any assumptions or corrections, such as tests of normality and adjustment for multiple comparisons
☐	☒	A full description of the statistical parameters including central tendency (e.g. means) or other basic estimates (e.g. regression coefficient) AND variation (e.g. standard deviation) or associated estimates of uncertainty (e.g. confidence intervals)
☐	☒	For null hypothesis testing, the test statistic (e.g. *F*, *t*, *r*) with confidence intervals, effect sizes, degrees of freedom and *P* value noted *Give P values as exact values whenever suitable.*
☐	☒	For Bayesian analysis, information on the choice of priors and Markov chain Monte Carlo settings
☒	☐	For hierarchical and complex designs, identification of the appropriate level for tests and full reporting of outcomes
☒	☐	Estimates of effect sizes (e.g. Cohen's *d*, Pearson's *r*), indicating how they were calculated

Our web collection on statistics for biologists contains articles on many of the points above.

Software and code

Policy information about availability of computer code

Data collection	All open source code and custom code used to collect the data is described in detail with versions in the methods section. Specifically, we used https://github.com/Secretloong/Cactus_Alignments_Tools, https://github.com/uym2/TreeShrink/tree/master/related_scripts, HAL v.2.3, PASTA v.1.8.5, TreeShrink v.1.3.1, MAFFT v7.149b, PHYLUCE v.1.6.3, Pargenes v.1.1.0, Modeltest-NG v.0.1.3, RAXML-NG v.0.9.0, RAXML-NG v.1.0.1, IQTREE v.1.6.12, IQTREE v2.0.4, newick-utilities v.1.6, ASTRAL-III v.5.14.5, FastRoot, CladeDate, MCMCtree v.4.9h, TreeCmp v.2.0, seqkit v.2.2.0, Pythia v. 1.0.0, PhyloMAd, CoalHMM, BayesTraits v.4, . We used the following R packages and functions: sn::st.mple v.2.0.0, phylolm, fastBM, evomap, missForest.
Data analysis	All open source code and custom code used to analyze the data is described in detail with versions in the methods section. Specifically, we used DiscoVista and functions implemented in base R for statistical analysis. Plotting for figures was done in R with dependencies contained in the scripts deposited in the data repository at https://doi.org/10.17894/ucph.85624f66-c8e5-4b89-8e8a-fe984ca89e4a

For manuscripts utilizing custom algorithms or software that are central to the research but not yet described in published literature, software must be made available to editors and reviewers. We strongly encourage code deposition in a community repository (e.g. GitHub). See the Nature Portfolio guidelines for submitting code & software for further information.

Data

Policy information about availability of data

All manuscripts must include a data availability statement. This statement should provide the following information, where applicable:

- Accession codes, unique identifiers, or web links for publicly available datasets
- A description of any restrictions on data availability
- For clinical datasets or third party data, please ensure that the statement adheres to our policy

The genome assemblies analyzed in this study and their whole genome alignment were part of the study by Feng et al. Nature 2020 and accession numbers are given as part of the Supplementary Data. Alignments, gene trees and species trees, in addition to data files produced for their analysis and scripts for plotting figures are available at https://doi.org/10.17894/ucph.85624f66-c8e5-4b89-8e8a-fe984ca89e4a. This repository also contains a file detailing contents and commands to use for individual and batch download of files. The study analyzed morphological trait data from AVONET (https://figshare.com/s/b990722d72a26b5bfead) and from https://doi.org/10.5061/dryad.fbg79cnw7, recombination rates for chicken (https://static-content.springer.com/esm/art%3A10.1186%2F1471-2156-11-11/MediaObjects/12863_2009_758_MOESM5_ESM.XLS), and time-calibrated species trees from Jarvis et al. Science 2014 (http://gigadb.org/dataset/101041) and Prum et al. Nature 2015 (Avian-TimeTree.tre from https://zenodo.org/records/28343).

Research involving human participants, their data, or biological material

Policy information about studies with human participants or human data. See also policy information about sex, gender (identity/presentation), and sexual orientation and race, ethnicity and racism.

Reporting on sex and gender	The study does not involve human participants or human data.
Reporting on race, ethnicity, or other socially relevant groupings	The study does not involve human participants or human data.
Population characteristics	The study does not involve human participants or human data.
Recruitment	The study does not involve human participants or human data.
Ethics oversight	The study does not involve human participants or human data.

Note that full information on the approval of the study protocol must also be provided in the manuscript.

Field-specific reporting

Please select the one below that is the best fit for your research. If you are not sure, read the appropriate sections before making your selection.

☐ Life sciences ☐ Behavioural & social sciences ☒ Ecological, evolutionary & environmental sciences

For a reference copy of the document with all sections, see nature.com/documents/nr-reporting-summary-flat.pdf

Ecological, evolutionary & environmental sciences study design

All studies must disclose on these points even when the disclosure is negative.

Study description	The study investigates phylogenetic relationships among bird species using whole genome sequences, spanning 363 species of birds.
Research sample	The loci for phylogenetic analysis were extracted from an existing whole genome alignment (https://doi.org/10.1038/s41586-020-2873-9) and analyzed using phylogenetic methods.
Sampling strategy	Sampling targeted at least one member for each taxonomic family of extant birds.
Data collection	We collected 159205 genetic loci from the whole genome alignment across the bird species using bioinformatic methods. For each locus we built a gene tree, which were summarized into species trees.
Timing and spatial scale	The data were extracted from the whole genome alignment at a single time point.
Data exclusions	We only excluded minimal amounts of data. We excluded fragmentary sequences, i.e. sequences shorter than 50% of the median length of all sequences of the locus because these fragmentary sequences can impact alignment accuracy and contain fewer parsimony informative sites than the remaining sequences. Secondly, we removed loci with fewer than 4 sequences as this is the minimum number of sequences needed to construct a tree.
Reproducibility	We performed bootstrapping to estimate statistical support on nodes of the best estimated tree. For subsetting analyses sampling a certain fraction of all gene trees, we performed 50 replicates to estimate amount of variation in the replicates.

Randomization	Decisions on groupings were based on bioinformatic cutoffs, therefore randomization was not relevant.
Blinding	Decisions on groupings were based on bioinformatic cutoffs, therefore blinding was not relevant.

Did the study involve field work? ☐ Yes ☒ No

Reporting for specific materials, systems and methods

We require information from authors about some types of materials, experimental systems and methods used in many studies. Here, indicate whether each material, system or method listed is relevant to your study. If you are not sure if a list item applies to your research, read the appropriate section before selecting a response.

Materials & experimental systems

n/a	Involved in the study
☒	☐ Antibodies
☒	☐ Eukaryotic cell lines
☒	☐ Palaeontology and archaeology
☒	☐ Animals and other organisms
☒	☐ Clinical data
☒	☐ Dual use research of concern
☒	☐ Plants

Methods

n/a	Involved in the study
☒	☐ ChIP-seq
☒	☐ Flow cytometry
☒	☐ MRI-based neuroimaging

Plants

Seed stocks	Not applicable.
Novel plant genotypes	Not applicable.
Authentication	Not applicable.

nature portfolio

Corresponding author(s): Stiller, Mirarab, Zhang

Last updated by author(s): Mar 6, 2024

Reporting Summary

Nature Portfolio wishes to improve the reproducibility of the work that we publish. This form provides structure for consistency and transparency in reporting. For further information on Nature Portfolio policies, see our Editorial Policies and the Editorial Policy Checklist.

Statistics

For all statistical analyses, confirm that the following items are present in the figure legend, table legend, main text, or Methods section.

n/a	Confirmed	
☐	☒	The exact sample size (*n*) for each experimental group/condition, given as a discrete number and unit of measurement
☐	☒	A statement on whether measurements were taken from distinct samples or whether the same sample was measured repeatedly
☐	☒	The statistical test(s) used AND whether they are one- or two-sided *Only common tests should be described solely by name; describe more complex techniques in the Methods section.*
☒	☐	A description of all covariates tested
☐	☒	A description of any assumptions or corrections, such as tests of normality and adjustment for multiple comparisons
☐	☒	A full description of the statistical parameters including central tendency (e.g. means) or other basic estimates (e.g. regression coefficient) AND variation (e.g. standard deviation) or associated estimates of uncertainty (e.g. confidence intervals)
☐	☒	For null hypothesis testing, the test statistic (e.g. *F*, *t*, *r*) with confidence intervals, effect sizes, degrees of freedom and *P* value noted *Give P values as exact values whenever suitable.*
☐	☒	For Bayesian analysis, information on the choice of priors and Markov chain Monte Carlo settings
☒	☐	For hierarchical and complex designs, identification of the appropriate level for tests and full reporting of outcomes
☒	☐	Estimates of effect sizes (e.g. Cohen's *d*, Pearson's *r*), indicating how they were calculated

Our web collection on statistics for biologists contains articles on many of the points above.

Software and code

Policy information about availability of computer code

Data collection	All open source code and custom code used to collect the data is described in detail with versions in the methods section. Specifically, we used https://github.com/Secretloong/Cactus_Alignments_Tools, https://github.com/uym2/TreeShrink/tree/master/related_scripts, HAL v.2.3, PASTA v.1.8.5, TreeShrink v.1.3.1, MAFFT v7.149b, PHYLUCE v.1.6.3, Pargenes v.1.1.0, Modeltest-NG v.0.1.3, RAXML-NG v.0.9.0, RAXML-NG v.1.0.1, IQTREE v.1.6.12, IQTREE v2.0.4, newick-utilities v.1.6, ASTRAL-III v.5.14.5, FastRoot, CladeDate, MCMCtree v.4.9h, TreeCmp v.2.0, seqkit v.2.2.0, Pythia v. 1.0.0, PhyloMAd, CoalHMM, BayesTraits v.4, . We used the following R packages and functions: sn::st.mple v.2.0.0, phylolm, fastBM, evomap, missForest.
Data analysis	All open source code and custom code used to analyze the data is described in detail with versions in the methods section. Specifically, we used DiscoVista and functions implemented in base R for statistical analysis. Plotting for figures was done in R with dependencies contained in the scripts deposited in the data repository at https://doi.org/10.17894/ucph.85624f66-c8e5-4b89-8e8a-fe984ca89e4a

For manuscripts utilizing custom algorithms or software that are central to the research but not yet described in published literature, software must be made available to editors and reviewers. We strongly encourage code deposition in a community repository (e.g. GitHub). See the Nature Portfolio guidelines for submitting code & software for further information.

Data

Policy information about availability of data

All manuscripts must include a data availability statement. This statement should provide the following information, where applicable:

- Accession codes, unique identifiers, or web links for publicly available datasets
- A description of any restrictions on data availability
- For clinical datasets or third party data, please ensure that the statement adheres to our policy

The genome assemblies analyzed in this study and their whole genome alignment were part of the study by Feng et al. Nature 2020 and accession numbers are given as part of the Supplementary Data. Alignments, gene trees and species trees, in addition to data files produced for their analysis and scripts for plotting figures are available at https://doi.org/10.17894/ucph.85624f66-c8e5-4b89-8e8a-fe984ca89e4a. This repository also contains a file detailing contents and commands to use for individual and batch download of files. The study analyzed morphological trait data from AVONET (https://figshare.com/s/b990722d72a26b5bfead) and from https://doi.org/10.5061/dryad.fbg79cnw7, recombination rates for chicken (https://static-content.springer.com/esm/art%3A10.1186%2F1471-2156-11-11/MediaObjects/12863_2009_758_MOESM5_ESM.XLS), and time-calibrated species trees from Jarvis et al. Science 2014 (http://gigadb.org/dataset/101041) and Prum et al. Nature 2015 (Avian-TimeTree.tre from https://zenodo.org/records/28343).

Research involving human participants, their data, or biological material

Policy information about studies with human participants or human data. See also policy information about sex, gender (identity/presentation), and sexual orientation and race, ethnicity and racism.

Reporting on sex and gender	The study does not involve human participants or human data.
Reporting on race, ethnicity, or other socially relevant groupings	The study does not involve human participants or human data.
Population characteristics	The study does not involve human participants or human data.
Recruitment	The study does not involve human participants or human data.
Ethics oversight	The study does not involve human participants or human data.

Note that full information on the approval of the study protocol must also be provided in the manuscript.

Field-specific reporting

Please select the one below that is the best fit for your research. If you are not sure, read the appropriate sections before making your selection.

☐ Life sciences ☐ Behavioural & social sciences ☒ Ecological, evolutionary & environmental sciences

For a reference copy of the document with all sections, see nature.com/documents/nr-reporting-summary-flat.pdf

Ecological, evolutionary & environmental sciences study design

All studies must disclose on these points even when the disclosure is negative.

Study description	The study investigates phylogenetic relationships among bird species using whole genome sequences, spanning 363 species of birds.
Research sample	The loci for phylogenetic analysis were extracted from an existing whole genome alignment (https://doi.org/10.1038/s41586-020-2873-9) and analyzed using phylogenetic methods.
Sampling strategy	Sampling targeted at least one member for each taxonomic family of extant birds.
Data collection	We collected 159205 genetic loci from the whole genome alignment across the bird species using bioinformatic methods. For each locus we built a gene tree, which were summarized into species trees.
Timing and spatial scale	The data were extracted from the whole genome alignment at a single time point.
Data exclusions	We only excluded minimal amounts of data. We excluded fragmentary sequences, i.e. sequences shorter than 50% of the median length of all sequences of the locus because these fragmentary sequences can impact alignment accuracy and contain fewer parsimony informative sites than the remaining sequences. Secondly, we removed loci with fewer than 4 sequences as this is the minimum number of sequences needed to construct a tree.
Reproducibility	We performed bootstrapping to estimate statistical support on nodes of the best estimated tree. For subsetting analyses sampling a certain fraction of all gene trees, we performed 50 replicates to estimate amount of variation in the replicates.

Randomization	Decisions on groupings were based on bioinformatic cutoffs, therefore randomization was not relevant.
Blinding	Decisions on groupings were based on bioinformatic cutoffs, therefore blinding was not relevant.

Did the study involve field work? ☐ Yes ☒ No

Reporting for specific materials, systems and methods

We require information from authors about some types of materials, experimental systems and methods used in many studies. Here, indicate whether each material, system or method listed is relevant to your study. If you are not sure if a list item applies to your research, read the appropriate section before selecting a response.

Materials & experimental systems

n/a	Involved in the study
☒	☐ Antibodies
☒	☐ Eukaryotic cell lines
☒	☐ Palaeontology and archaeology
☒	☐ Animals and other organisms
☒	☐ Clinical data
☒	☐ Dual use research of concern
☒	☐ Plants

Methods

n/a	Involved in the study
☒	☐ ChIP-seq
☒	☐ Flow cytometry
☒	☐ MRI-based neuroimaging

Plants

Seed stocks	Not applicable.
Novel plant genotypes	Not applicable.
Authentication	Not applicable.